Downsized Flexible Capacitive Strain Sensing Filament and Its Application in Knee Angle Tracking During Walking

by

Wanhaoyi Geng

B.A.Sc., University of British Columbia, 2016

Thesis Submitted in Partial Fulfillment of the
Requirements for the Degree of
Master of Applied Science

in the
School of Engineering Science
Faculty of Applied Science

SIMON FRASER UNIVERSITY
Fall 2019

Approval

Name:	**Wanhaoyi Geng**
Degree:	**Master of Applied Science (Engineering Science)**
Title:	**Downsized Flexible Capacitive Strain Sensing Filament and Its Application in Knee Angle Tracking During Walking**
Examining Committee:	**Chair:** Michael Sjoerdsma Senior Lecturer
	Carlo Menon Senior Supervisor Professor
	Mohammad Narimani Supervisor Lecturer
	Michael Adachi Internal Examiner Assistant Professor
Date Defended/Approved:	December 18, 2019

Ethics Statement

The author, whose name appears on the title page of this work, has obtained, for the research described in this work, either:

a. human research ethics approval from the Simon Fraser University Office of Research Ethics

or

b. advance approval of the animal care protocol from the University Animal Care Committee of Simon Fraser University

or has conducted the research

c. as a co-investigator, collaborator, or research assistant in a research project approved in advance.

A copy of the approval letter has been filed with the Theses Office of the University Library at the time of submission of this thesis or project.

The original application for approval and letter of approval are filed with the relevant offices. Inquiries may be directed to those authorities.

Simon Fraser University Library
Burnaby, British Columbia, Canada

Update Spring 2016

Abstract

Assistive Rehabilitation technologies have been a prominent research topic in recent years for patients who suffer from impaired lower extremity motor abilities. Continuous tracking of knee movement can provide valuable insight into the effectiveness of therapeutic or surgical interventions such as improvements in range of motion or stability over the course of the treatments. Video-based motion tracking is an industry standard for motion tracking, but its usage is limited in a clinical setting due to its prohibitive cost and space requirement. This study proposes a downsized flexible capacitive strain sensing filament that can be weaved into textiles to achieve in situ motion tracking. Its effectiveness is shown in a knee joint angle tracking with video-based motion capture as reference. Sensor-predicted knee angle is 99% accurate when compared to the reference with root mean square error of 1.79 degrees. An improved sensor is also fabricated and characterized to show enhanced performance.

Keywords: Capacitive Sensing, Strain Sensing, Motion Tracking, Knee Joint

Table of Contents

Approval ii
Ethics Statement iii
Abstract iv
Table of Contents v
List of Tables vii
List of Figures viii

Chapter 1. Introduction 1
1.1. Motivation 1
1.2. Objectives 6
1.3. Thesis Layout 7

Chapter 2. Literature Review 8
2.1. Introduction to Capacitors 8
2.2. Capacitive Strain Sensors 10
2.2.1. Parallel Plate Capacitive Strain Sensors 11
2.2.2. Interdigitated Capacitive Strain Sensors 15
2.2.3. Twisted Double Helix Capacitive Strain Sensors 16
2.2.4. Woven Capacitive Fabric 17
2.2.5. Cylindrical Capacitors 18

Chapter 3. Prototype Sensor Fabrication and Smart Knee Brace Integration With Knee Angle Monitoring for Walking Experiment 21
3.1. Types of Elastomer 21
3.1.1. Thermoplastic Elastomer 21
3.1.2. Thermoset Elastomer 21
3.2. Factors Affecting Sensor Performance 22
3.2.1. Mechanical Properties 22
3.2.2. Dielectric Layer Thickness 24
3.2.3. Dielectric Constant 25
3.2.4. Equivalent Series Resistance 25
3.3. Initial Design with Silicone Tube 25
3.4. Material Choice for Prototype Sensor 26
3.5. Sensor Fabrication 27
3.6. Knee Brace Prototype and Knee Angle Monitoring for Walking Test 31
3.6.1. Preliminary Bending Stage Test 31
3.6.2. Knee Anatomy and Sensor Placement 33
3.6.3. Sensor Embedding: Knee Brace for In Situ Knee Joint Angle Monitoring 34
3.6.4. Calibration Method and Real-time Knee Angle Tracking for Walking 40
3.7. Chapter Conclusion 43

Chapter 4. Capacitance Data Collection Circuitry 44
4.1. DC Direct Charge Method 44

4.2. LC Tank Circuit Resonant Frequency Modulation 46
4.3. Charge Balancing Circuit 51
4.4. 555 Timer Astable Multivibrator Circuit 53
4.5. Chapter Conclusion 55

Chapter 5. Characterization of Improved Sensor 57
5.1. Improved Capacitive Sensing Filament 57
5.2. Characterization 57
5.2.1. Stress-Strain Curve 58
5.2.2. Large Strain Test 59
5.2.3. Hysteresis Curve 60
5.2.4. Frequency Performance 61
5.2.5. Long-term Cyclic Stability 63
5.2.6. Static Load 63
5.2.7. Random Tracking 64
5.3. Chapter Conclusion 65

Chapter 6. Conclusion 67
6.1. Conclusion 67
6.2. Limitation 68
6.3. Future Work 68

Bibliography 69

List of Tables

Table 1 - Advantages and Disadvantages of the explored capacitance measurement circuits 55
Table 2 - Objectives and Accomplishment 67

List of Figures

Figure 1 - Electrogoniometer with two plastic endblocks 2
Figure 2 - Typical resistive sensor response to a step-hold-release strain test 4
Figure 3 - Typical capacitive sensor response to a step-hold-release strain test 5
Figure 4 - A realistic model for a capacitor 9
Figure 5 - A parallel plate DEAP actuator 10
Figure 6 - A parallel plate capacitive strain sensor. 12
Figure 7 - A smart knee brace for joint angle monitoring with 3 parallel plate capacitive sensor embedded 13
Figure 8 - A single layer, interdigitated capacitive strain sensor 15
Figure 9 - A twisted double helix capacitive strain sensor. 16
Figure 10 - A capacitive fabric used for strain and pressure sensing. 17
Figure 11 - A encapsulated ionic liquid capacitive sensor. 19
Figure 12 - Stress-strain curve of a polymer and parameters associated with its mechanical property 23
Figure 13 - Fabrication procedure for the dip coated sensor 28
Figure 14 - Dip coating apparatus: Vertically placed synringe pump, clamped tweezer on linear stage, and vial for dip coating solution 29
Figure 15 - a) Dielectric layer coated with Hytrel 3078 in Dichloromethane solution showing porous structure. b) SEBS dielectric peeling and cracking after long exposure in SEBS-Cyclohexane solution 30
Figure 16 - Hysteresis curve for prototype sensor showing non-linear behavior 31
Figure 17 - Bending stage test setup 32
Figure 18 - Bending stage test capacitance reading for different stage flexion angles 33
Figure 19 - Anatomy of human knee. 34
Figure 20 - Sensor embedding by sewing technique to allow stretching 35
Figure 21 - Sensor embedding through weaving in knee brace with metal snap buttons and conductive thread 36
Figure 22 - Reflective marker placement for motion tracking system 37
Figure 23 - Top: Sensor reading for simple knee flexion and extension. Bottom: Sensor reading versus Knee angle data points used for polynomial fitting 38
Figure 24 - Sensor predicted knee angle for simple flexion and extension 39
Figure 25 - Video screen capture showing ionic liquid capacitive strain sensor showing large error when knee is fully extended Top right shows the capacitance reading, bottom left shows the resistive reading. 40
Figure 26 - Calibration process, protractor measuring marker (knee) angle 41
Figure 27 - Calibration measured angle versus knee brace sensor reading and fitted polynomial 41

Figure 28 - Walking Test a: Comparison between sensor predicted angle and motion capture reference angle; b: Predicted baseline before walking test, c: Predicted bottom line after the walking test 43
Figure 29 - Typical equivalent series resistance of the sensor prototype during a triangular strain 45
Figure 30 - Capacitance data collected by the DC direct charge method..... 46
Figure 31 - A parallel LC resonant circuit..... 47
Figure 32 - A parallel LC resonant circuit with sensor attached 48
Figure 33 - Changes in resonant frequency caused by increasing capacitance assuming minimal ESR. From black is with small capacitance to Green is with large capacitance..... 48
Figure 34 - Effect of high ESR on the resonance frequency, changing capacitance no longer change the frequency 49
Figure 35 - Changes in resonance frequency while increasing sensor capacitance and ESR simultaneously 50
Figure 36 - Sensor Capacitance captured by FDC2212EVM showing reverse behaviour and resistive hysteresis and creep..... 50
Figure 37 - Sigma Delta Analog to Digital Converters..... 51
Figure 38 - Sigma-Delta Analog-to-Digital Converter in capacitance measurement (charge balancing) mode..... 52
Figure 39 - AD7745 range extension circuit..... 52
Figure 40 - Sensor data captured by the AD7745..... 53
Figure 41 - 555 Timer Astable Multivibrator Circuit..... 54
Figure 42 - Sensor capacitance captured by the 555 Timer Astable Multivibrator circuit 55
Figure 43 - Stress-strain comparison of bare Hytrel 3078 filament and the coated sensor 58
Figure 44 - Sensor reading in large 100% strain showing considerable plastic deformation 59
Figure 45 – Hysteresis Curve for the improved sensor in its 30% strain linear region 61
Figure 46 Top: Sensor Reading for different frequencies Bottom: Maximum peak-peak amplitude reached in each frequency band 62
Figure 47 - Cyclic testing for sensor repeatability and material fatigue 63
Figure 48 - Sensor reading in step-up and step-down static load test..... 64
Figure 49 - Sensor predicted displacement compared to reference displacement logged by Instron tensile tester..... 65

Chapter 1. Introduction

1.1. Motivation

Assistive Rehabilitation technologies have been a prominent research topic in recent years for patients who suffer from impaired lower extremity motor abilities after a Spinal Cord Injury or a stroke. Continuous tracking of knee movement can provide valuable insight into the effectiveness of therapeutic or surgical interventions such as improvements in range of motion or stability over the course of the treatments [5,65]. Tracking data can also serve as feedback for rehabilitation technologies such as Functional Electrical Stimulation and Galvanic Vestibular Stimulation [26,29]. Current methods for joint motion tracking for physiotherapy include analog and digital goniometers, markerless video motion capture, and most commonly, unaided visual inspection by a physiotherapist. [24]

Analog goniometers are easy to use, affordable and offers good intrarater repeatability [57]. An individual generally follows the same measurement procedures and placement of the analog goniometer and thus is able to produce repeatable measurement results. Different examiners however may follow different measurement procedures and different goniometer placement resulting in low interrater repeatability. Analog goniometers are widely used in passive range of motion (PROM) examination where a joint is moved by the physiotherapist or a machine that requires no patient effort. The analog goniometer is used to record the static angle held by the machine or by the physiotherapist. However, it is challenging to perform active range of motion (AROM) examination with an analog goniometer since holding certain postures with maximum flexion or extension is not always possible.

Digital goniometers use technologies such as still-image processing and can be found in smart phone apps (such as DrGoniometer) [51]. A still image of a flexed joint is taken by the smart phone camera and examiner measures the joint angle by placing traces on the image taken. The still-image processing shares the same disadvantage as the analog goniometers since the repeatability largely depend on the location of trace placement by the specific examiner. Some types of digital goniometer use accelerometer and gyroscope which suffer from an accumulated drift error [11,19,34]. A more recent and more advanced version of the digital goniometer is the electrogoniometer (Figure.1)

utilizing half-bridge strain gauges and can sense bending in two planes perpendicular to each other [33].

Figure 1 - Electrogoniometer with two plastic endblocks
Adapted from "Twin-Axis Electrogoniometers for Joint Movement Analysis," Biometrics Ltd. Retrieved November 10th, 2019, from http://www.biometricsltd.com/goniometer.htm

The electrogoniometer can provide continuous angle measurement of a joint especially useful in AROM, but a torsional displacement in one of its plastic end blocks will result in strain in both of its opposing strain gauges causing measurement errors known as crosstalk errors [27].

Markerless video-based motion tracking provides a more holistic approach to analyzing joint movement and allows the tracking of multiple joints at once with a tracking software automatically identifying the biomechanics of the examined subject. The markerless approach is less accurate than a traditional multi-camera marker-based video motion tracking system but the results produced are comparable to their marker-based approach for certain motions [25].

The marker-based multi-camera video motion capture system is an industry standard for motion tracking and offers the standard in many biomechanics researches. Both camera-based systems suffer from problem such as occlusion and can only be used in spaces with minimal obstruction. Video-based motion tracking systems are also considerably more expensive, and less portable than the goniometers.

To achieve continuously motion tracking outside of a clinical setting, portable and wearable solutions have been developed over the past decades to achieve in situ motion tracking. These include rigid electronic sensors such as accelerometers, gyroscopes, and Inertial Measurement Unit [20] (which include a combination of the aforementioned sensors). However, despite their increasingly small size over the years these rigid sensors are still uncomfortable to wear. With the lack of a positional reference some of these sensors often suffer from an accumulated error that worsen over time [20]. Different methods have been developed to correct this drift over time problem but that often involves adding extra sensors such as magnetometers to provide a positional reference [20] resulting in even higher sensor density and further decrease in comfort.

With the rising popularity in smart materials and textiles in recent years, soft wearable sensors are now being used to monitor joint movement. When embedded in textiles these wearable sensors are promising to allow long term joint movement monitoring in the context of home rehabilitation. Researches have shown promising results in using soft polymeric strain sensors embedded in garments to detect human motion [2,9,17,23]. These techniques can achieve localized motion tracking [2,49] and do not suffer from problem such as occlusion often faced by conventional video-based motion tracking [24]. These soft sensors transduce geometric deformations into changes in some measurable electrical signals, which can be used to calculate joint angles to reconstruct body posture. The increased comfort level offered by these soft wearable sensors allows extended monitoring time and a more holistic view of patient performance doing various activities over the day.

The soft polymeric strain gauges can be divided into different subclasses depending on their sensing modality. Resistive polymeric strain gauges and capacitive polymeric strain gauges are two of the most researched types of these soft strain sensors and each offers their unique advantage and disadvantage suitable for different applications.

Resistive soft strain sensors [17,43,44,46] utilize conductive particles dispersed in a polymer matrix or conductive liquid (ionic liquid) encapsulated in polymer and measures the change in resistance caused by piezoresistivity as a result of applied mechanical stress. The performance of these sensors can be modelled by a viscoelastic model and often suffer from resistance drift over time under static load caused by material creep [35,40,55]. The initial response to a sudden strain will cause a sudden increase in stress

as part of the elastic response of the material, this will produce a spike in resistance depending on strain rate. The spike will quickly recover to a certain degree through elastic recovery and then continue to recover at a slower rate when the strain is held constant and the viscous effect causes stress to relax over time [55]. Resistive sensors suffer from hysteresis that cause the sensor to have a slow recovery of its initial baseline resistance after strain is removed. The hysteresis is the result of difference in time needed for the breakdown and reformation of contacts between the conductive particles in the polymer matrix and the inherent hysteresis of elastomer loading [35].

Resistive sensors involve a relatively simpler fabrication process such as extrusion, electrospinning or coating, and generally involves less complicated readout circuitry [21]. A typical response of the resistive sensor to a step-hold-release strain cycle [35,40] is shown in Figure. 2:

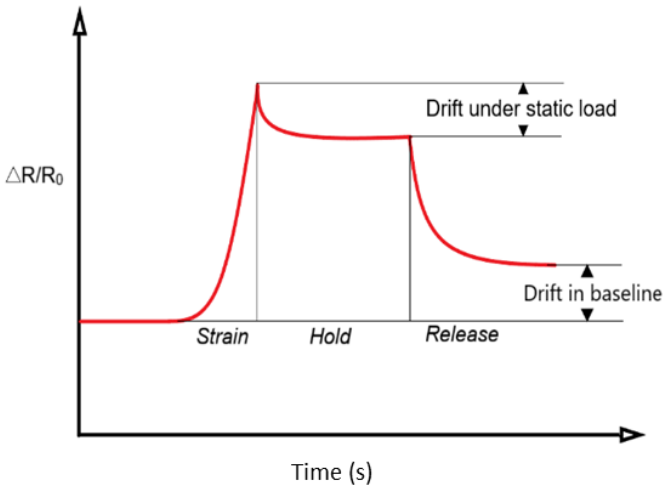

Figure 2 - Typical resistive sensor response to a step-hold-release strain test

The drift resulted in low repeatability in readings, and stable and repeatable readings are essential for accurately predicting the current strain% for the sensor for motion tracking purposes. For applications involving motion classification however, such as gesture/posture detection, where the accurate angle of the involved joints is not the primary concern, resistive strain sensors can perform very well. Their large gauge factor (up to 13920 reported [15]), which measures the amount of electric signal change per unit strain, results in large changes in electrical resistance that, despite drift and hysteresis in the system, can still establish clear decision boundaries useful for classification. Researches have shown success in detecting hand gestures using

resistive sensors embedded on a glove[35] and detecting gait cycles with resistive sensors embedded on lower body garments [10].

Soft capacitive sensors rely on geometric changes in its electrode area and dielectric layer thickness caused by applied strain which in turn produces a change in its capacitance [43]. The shift from relying on sensor material's internal stress (as for the case of piezoresistivity) to its geometry allows the capacitive sensor to have a bore direct correlation with the sensor material's resilience and elasticity, and suffer less from hysteresis caused by material creep and its time-dependent behaviour. A typical response of the capacitive sensors [44] to a strain-hold-release cycle is shown in Figure 3:

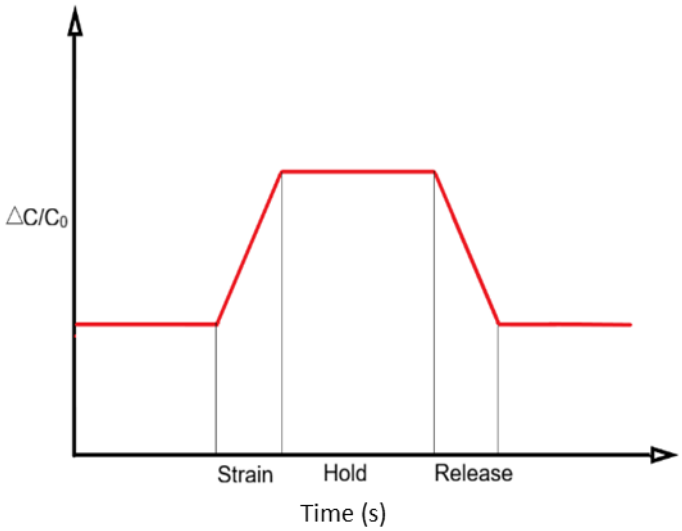

Figure 3 - Typical capacitive sensor response to a step-hold-release strain test

A steady reading under static strain and reliable recovery to the original baseline allow capacitive soft strain sensors to produce repeatable results within the elastic region of the material that is suitable for dynamic application such as motion tracking where an accurate angle is key to knowing the orientation of the tracked joints. A common structure of the sensor is that of a soft parallel plate capacitor with flexible polymeric electrodes sandwiching a dielectric layer [44,49,56]. Parallel plate soft capacitive sensors are shown to be able to accurately track joint angles [49]. However, parallel plate capacitive sensors have limited ways to be embedded into garments and they need enough conductive electrode area for a sizeable signal resulting in bulkiness in the sensor system. To downsize these sensors to facilitate embedding into textile

applications, recent researches have grown interest in soft cylindrical capacitors [23,47,54]. Unlike parallel plate capacitors, whose capacitance is governed by the conductive electrode area and thickness of the dielectric layer, multilayer cylindrical soft capacitors' capacitance is affected by the ratio of its outer and inner radius of the dielectric layer. The reliance on radius ratio allows the sensor to be down-sized without suffering a decrease in baseline signal produced and allows the production of thin capacitive filament that can be sewn, threaded or weaved into garments for enhanced integration and aesthetics. Reduced size also allows for higher sensor density in areas where the motion is complicated to facilitate machine learning.

In order to obtain comparable performance to existing technologies such as goniometers and video-based motion tracking, wearable soft strain sensors need to satisfy certain metrics. Human motor functions can reach a frequency as high as 10Hz [19], and hence the sensor used in human motion tracking must respond well at twice the maximum frequency (20Hz). Considering an indoor setting where the person maybe stationary for long periods of time, it is desirable for the sensor to respond well to static load with negligible drift (<0.1%) [2]. For outdoor motion tracking, the sensor should be robust to prevent material fatigue caused by extensive cyclic straining (<0.3% change in signal/1000 cycles [54]). The sensor should have stable capacitance across a wide range of temperature and humidity since factors such as weather and body sweat could potentially cause a change in sensor signal.

1.2. Objectives

This study has the following objectives:

Objective 1: To develop a reliable capacitive filament sensor with low drift (<0.1%) [2] under static load, good cyclic performance (<0.3% change in reading over 1000 cycles) [54] and good linearity (R^2 > 0.9995 [44]). The baseline of the sensor needs to be larger than 150pF to minimize effect of parasitic capacitance and achieve higher signal-to-noise ratio as reported in [2].

Objective 2: Develop reliable data collection circuit prototype for the sensor that produces repeatable result that can be used for motion tracking.

Objective 3: To monitor real-time knee angle with the sensor embedded in garments. Achieve 96% [49] accuracy when compared with video-based motion capture system.

1.3. Thesis Layout

The thesis will be organized as follows:

In Chapter II there will be a thorough literature review on current wearable soft capacitive strain gauge technologies and their applications. Chapter III explains the fabrication process of a prototype capacitive strain sensor and its integration in textiles and reports the result of a comparison between sensor and video motion capture measured knee angle in a walking test while wearing a knee brace with the sensor embedded. Chapter IV covers the different electronic circuits designed for data collection and their respective strengths and weaknesses. Chapter V covers an improved version of the prototype sensor and its rigorous characterization showing improved performance.

Chapter 2. Literature Review

2.1. Introduction to Capacitors

The soft capacitive strain senor is, above all else, a capacitor. The very beginning of the capacitive technology can be traced back to the 1745s when the German Ewald Georg von Kleist invented the Leyden jar which was later improved by Benjamin Franklin, who made flat capacitors consisting of a sheet of glass in between foil electrodes. Faraday later proposed the concept of dielectric constant and invented the first practical fixed and variable capacitor, and his name is used as the unit for capacitance to recognize his immense contribution to capacitor technologies [28].

A capacitor consists of two conductive electrodes separated by an insulator known as the dielectric. Although theoretically any non-conductive material can be used as the dielectric, types of dielectric used determines whether the capacitor's suitable application is for high frequency or high voltage applications.

A capacitor stores electrical charge in the form of an electrostatic field between the electrode when a voltage is applied to its terminals, as more charge is being stored, the field grows in strength and that energy is depleted when the capacitor is discharged. Capacitance is defined as the ratio between the amount of electric charges stored and the potential difference between the electrode:

$$C = \frac{Q}{V}$$

Where *Q* is the amount of charge stored with a unit of coulomb, *V* is the potential difference between the electrodes (the capacitor will be charged to the power supply voltage after a period of time that is determined by the time constant of the capacitor).

A theoretical, or ideal capacitor has only a capacitive component, but such capacitors do not exist in real-life applications. A realistic model for a capacitor is illustrated in Figure.4

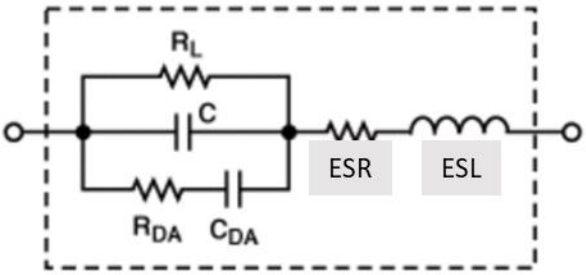

Figure 4 - A realistic model for a capacitor

These parasitic components make up a real capacitor and can have a significant impact on capacitor performance.

- R_L is the leakage resistance of the capacitor C. In an ideal capacitor, the charge stored on the capacitor will only vary in response to external current flow. The leakage resistance will cause the capacitor to lose charge at a rate determined by the RC (in this case R_LC) constant and produce a leakage current, that is the result of current flowing through the dielectric when a voltage is applied.

- R_{DA} and C_{DA} combined constitutes the Dielectric Absorption characteristics of a capacitor, which is a capacitor's inability to fully release all its stored energy. The energy that is not released could show as a percentage of the original charge regained after fully discharging a capacitor. The hysteresis-like behaviour is the result of dipole movements in the dielectric. The electrostatic field present in a charging capacitor will orient the dipoles in the dielectric to align with the electric field lines, and these twisted dipoles store energy compared to their unturned state. Free electrons also move within the dielectric and store energy chemically. These combined contribute to the energy regained after discharging a capacitor.

- ESR is the equivalent series resistance of the capacitor and consists of the lead resistance, electrode resistance and dielectric loss. Although the model suggests that equivalent series resistance is constant with respect to frequency, in reality the ESR does change at high AC frequency because of the skin effect where current density is higher near the surface of the conductor. Equivalent Series Resistance causes a capacitor to dissipate power.

- ESL is the equivalent series inductance of the capacitor and results from the inductance of capacitor leads in series with the equivalent inductance of the capacitor electrodes. The equivalent series inductance and equivalent series resistance can impact sensor performance at high frequency due to an amplified resonance.

Some of these parasitic effects of a realistic capacitor will have an impact on capacitive strain sensing and its data collection circuits and will be discussed in later chapters.

2.2. Capacitive Strain Sensors

The idea of using a deformable soft capacitor to measure strain have been proposed for decades and many different designs and material usage have been explored to serve different purposes. It originated from researchers studying the effect of an electric field being applied to a dielectric elastomer, which would cause a strain response in the dielectric elastomer that was proportional to the electric field being applied. [34] This mechanism provided ground for developing soft actuators and sparked development of various deformable soft capacitors which soon became more than just actuators when the reversal of this mechanism could serve as a strain sensor.

Dielectric Electroactive Polymer (DEAP) are used in these soft actuators, electrostatic force resulting from high voltage being applied to the electrodes will squeeze the DEAP material to cause an actuation [50] as illustrated in Figure.5

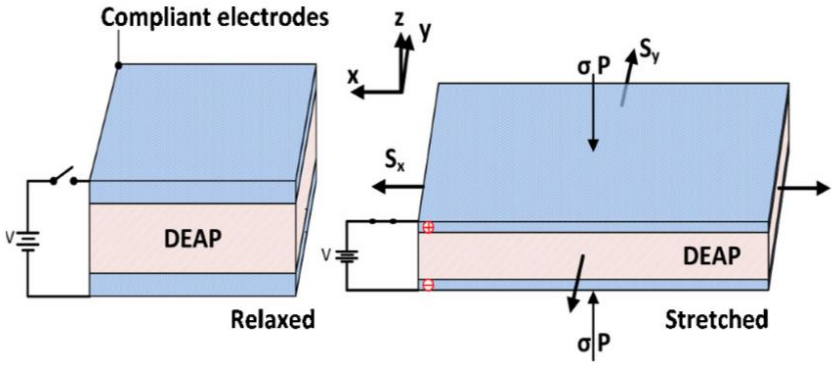

Figure 5 - A parallel plate DEAP actuator
Adapted from "Modeling and control of hysteresis for DEAP actuator," by B.N.M. Truong, October 15th, 2013, Sensors and Actuators A: Physical, volume 21, page 193-206

These membrane actuators as shown in Figure.5 can be rolled up to achieve axial extension (along the rolling axis) [41] and function as a strain sensor that is based on parallel plate capacitance despite its tubular shape.

In more recent years, these soft polymeric capacitors became smaller in size to serve specifically as wearable strain sensors or to act as feedback sensors for soft robotics. In this chapter a thorough literature review will be conducted based on different structures current researches on wearable capacitive strain sensing are exploring.

2.2.1. Parallel Plate Capacitive Strain Sensors

As the simplest structure to produce a capacitance, the parallel plate structures are largely popular in current research. Most of these parallel plate soft capacitive strain sensors consists of thin polymeric films layered together with two conductive polymeric electrodes sandwiching a dielectric layer with its capacitance given by

$$C = \epsilon \frac{A}{d}$$

Where ϵ is the relative permittivity of the dielectric material, *A* is the conductive area of the electrodes, and *d* is the distance between the electrodes (thickness of the dielectric layer). The performance of these sensors relies upon the mechanical property of the backbone polymer used, and on the electrode conductivity stability and the dielectric characteristics of the dielectric material.

Conductive polymeric electrodes are often made through dispersion of a conductive nanoparticle or metal nanowires in an elastomeric substrate. One example is the work of Shintake et al. [44] Their sensors used Carbon Black – Elastomer composite as compliant electrodes. Carbon Black was dispersed into a silicone matrix (Ecoflex 30) at 10 wt% to form the electrode composite and the sensor was produced through a layer by layer casting process. The Ecoflex silicone material is used both as the protective base/seal and as the dielectric layer. Electrical connection was achieved through a laser ablation process on the electrode to curve out a specific pattern that isolate and expose the contact point for the top and the bottom electrode as shown in Figure.6.

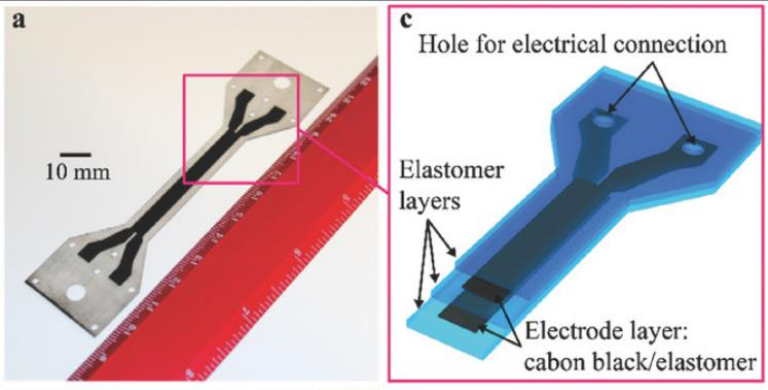

Figure 6 - A parallel plate capacitive strain sensor.
Adapted from "Ultrastretchable Strain Sensors Using Carbon Black-Filled Elastomer Composites and Comparison of Capacitive Versus Resistive Sensors," byJ. Shintake et al., 2018, Advanced Materials Technologies, volume 3

The sensor demonstrated high linearity (R^2 = 0.9995) and cyclic repeatability (-1.7% at 0% strain and -10.8% at 200% strain after 10100 cycles of 200% strain) for up to a strain of 500%.

Cai et al. [8] developed similar sensors by transferring Carbon Nanotube film onto both sides of a silicone (Dragon Skin 30) substrate and then sealed with silicone glue (PDMS) after establishing electrical contact with silver paste and copper wire. The resulting sensor was characterized to have capacitance linearly proportional to strain up to 300% with very low hysteresis

Totaro et al. [49] developed a 5-layer capacitive strain sensor that employed two capacitors parallel with each other by using three electrode layers and two dielectric layers and achieving an electrode-dielectric-electrode-dielectric-electrode structure. The sensing reading is the sum of the two individual capacitors for a larger baseline. Totaro et al. demonstrated sensor performance in knee joint angle monitoring by attaching three sensors along the sagittal axis across the kneecap in an attempt to achieve higher correlation with the bending angle through exploiting sensor redundancy as shown in Figure.7

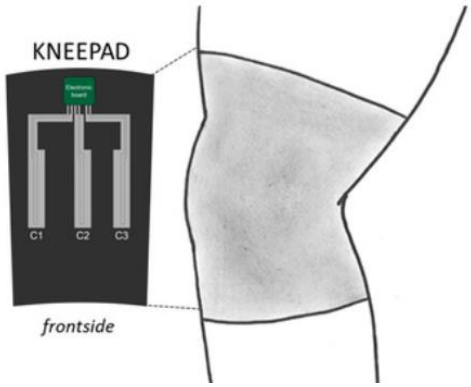

Figure 7 - A smart knee brace for joint angle monitoring with 3 parallel plate capacitive sensor embedded

Adapted from " Soft Smart Garments for Lower Limb Joint Position Analysis," by M. Totaro et al., 2017, Sensors, volume 17

Totaro et al. reported angle measurement error of less than 4 degrees for simple flexion-extension using a polynomial fitting method.

Despite using a dispersion method, the above sensors did not see a significant reinforcement of the elastic modulus (young's modulus) as reported in [42] by Sekitani et al., which would drastically hinder the sensor's mechanical properties because of a stiffening effect. This could be explained by the material usage in both cases as the Ecoflex and Dragon Skin material from Smooth-On was a silicone rubber with platinum catalyzed addition curing that facilitates the crosslinking reaction of the material to form a three-dimensional network [70,71]. When compounded with a relatively low loading of the conductive nanoparticle, the effect of a reinforced elastic modulus was not evident in the above studies.

To combat the reinforcing effect, Cohen et.al [14] produced parallel plate capacitive sensors through the direct transfer of Single Walled Carbon Nanotubes (SWCNT) to a plasma treated hydrophobic pattern on both sides of a silicone substrate. The sensor demonstrated high linearity up to 100% strain and less than 3% drift after 3000 cycles of 100% strain and the sensor was demonstrated to function as an accurate angle transducer for a four-bar linkage.

While most parallel plate capacitive sensors exhibit gauge factors less than or close to 1 as predicted by the theoretical formula

$$C = \epsilon \frac{(1+\varepsilon) l_0 (1 - v_{electrode}\varepsilon) w_0}{(1 - v_{dielectric}\varepsilon) d_0}$$

Where ε is the applied strain, l_0, w_0, and d_0 is the initial length, width, and thickness respectively, $v_{electrode}$ and $v_{dielectric}$ is the Poisson ratio for the electrode and dielectric material respectively.

It can be seen that when $v_{electrode} \approx v_{dielectric}$, which is the case for most elastomer that is assumed to be isotropic and incompressible with a Poisson ratio of close to 0.5, the above equation evaluates to

$$C = \epsilon \frac{(1+\varepsilon) l_0 w_0}{d_0} = (1+\varepsilon)\epsilon \frac{A}{d} = (1+\varepsilon) C_0$$

And thus, results in a gauge factor of 1. The usage of stiff electrode material with a Poisson ratio of less than 0.5 can however achieve a higher than 1-gauge factor not commonly achievable by soft capacitive strain sensors.

One example was the work of Nur et al. [36] that utilized gold films as the electrode. Even though gold films were inherently brittle and could fracture with 1% of applied strain. Nur et al applied thin gold film onto a 50nm parylene film that was later transferred onto a pre-strained dielectric layer. The Gold-Parylene film formed spontaneously buckled electrode that could sustain up to 140% strain and reported gauge factor of 3.05. A decrease in performance for cyclic loading was reported as a noticeable decrease in signal amplitude was present after 1000 cycles of 50% straining which is explained by the unrecoverable micro cracks of the fatigued gold electrode.

Atalay et al. [2] developed textile-silicone composite parallel plate capacitive sensors by gluing stretchable knitted conductive fabric onto both sides of a silicone substrate as electrodes and achieved a gauge factor of 1.23. While having comparable performance in terms of linearity and repeatability with aforementioned sensors up to a strain of 100%.

2.2.2. Interdigitated Capacitive Strain Sensors

While appearing as a thin film capacitor, interdigitated capacitors do not rely on a multi-layered structure but rather utilizes single-layer, interdigitated electrodes to achieve a capacitance as illustrated in Figure.8.

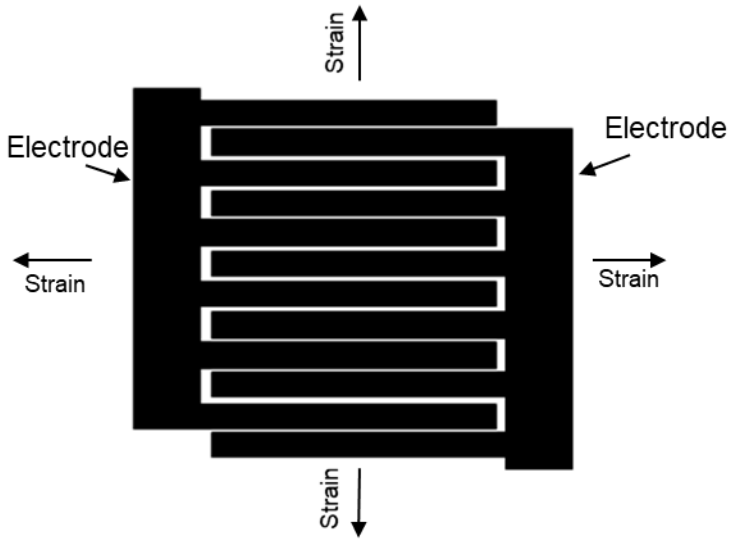

Figure 8 - A single layer, interdigitated capacitive strain sensor

When stretched along the interdigitated finger direction, the gap between fingers decrease and the overlapping length of the fingers increase, resulting in an increase in capacitance. This structure can also sense strain perpendicular to the finger directions as the gap between the fingers increase and the overlapping length of the fingers decrease.

Atalay et al. [52] developed interdigitated capacitive strain sensor through laser cutting of conductive fabric glued to a silicone substrate into the electrode pattern. The sensor has good linearity but suffered a 3% decrease in signal amplitude after 500 cyclic testing of 50% straining.

Kim et al. [30] deposited electrode pattern with Silver Nanowires onto a PDMS substrate through a capillary force lithography method. The resulting sensor demonstrated a gauge factor larger than 1 in the direction perpendicular to the finger direction but has noticeably different load-unload characteristic.

The most noticeable advantage of the interdigitated structure, aside from the ease of batch manufacturing through film casting and laser cutting much similar to that of a parallel-plate sensor, is that the electrodes presiding in the same plane allows the sensor to be immune to applied pressure perpendicular to the electrode. This pressure is often present and noticeable if the sensors are used in bending detection and the bent joint is applying pressure on the sensor.

2.2.3. Twisted Double Helix Capacitive Strain Sensors

Filament-like capacitors are developed by twisting stretchable conductive thread with an outer insulating layer together (Figure.9) to achieve a capacitance.

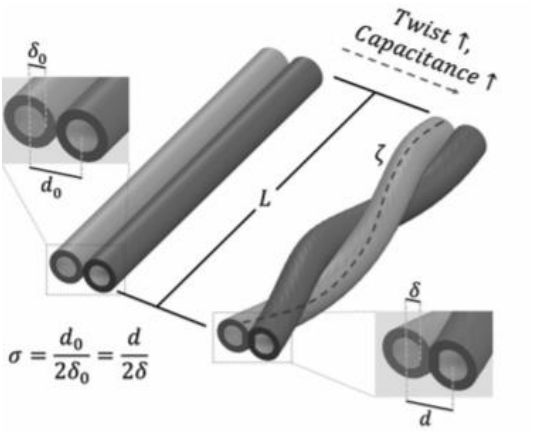

Figure 9 - A twisted double helix capacitive strain sensor.
Adapted from " Stretchable Capacitive Sensors of Torsion, Strain, and Touch Using Double Helix Liquid Metal Fibers," by C. Cooper et al., 2017, Advanced Functional Materials, volume 27

This has been one of the least explored structure as a capacitive strain sensor and few reports were found utilizing this structure. Cooper et al. [15] proposed this structure by intertwining thin liquid-metal-filled elastomeric tubes. An increase in torsional level (in radians/unit length) would increase the baseline reading. Elongation along the length of the sensor resulted in an increase in capacitance because of larger(longer) contact area between the two tubes which was offset to some degree by a decrease in the torsional level. The sensor performed better with high initial torsional level at 1571 radians/meter, but the baseline reading was around 1pF/cm which was noticeably lower than the aforementioned sensors. The sensor was also able to sense torsional strain because of

its structure but the inability to separate this from changes caused by elongational strain rendered this a disadvantage rather than an advantage.

2.2.4. Woven Capacitive Fabric

The capacitive sensing technology can be achieved through a fabric based form where each thread used has a conductive core/layer and is coated on the outside with an insulating material, thus when woven together, each intersection of the woven grid functions as a small capacitor and strain can be calculated by analyzing the capacitance between each pair of intersecting threads.

One example is the work of You et al [63] here a cotton thread was made into a conductive thread after nickel deposition and coated with a dielectric layer made from graphene-oxide-doped polyurethane. This composite thread was then core-spun onto an elastic thread and woven together to achieve a capacitive sensing fabric (Figure.10).

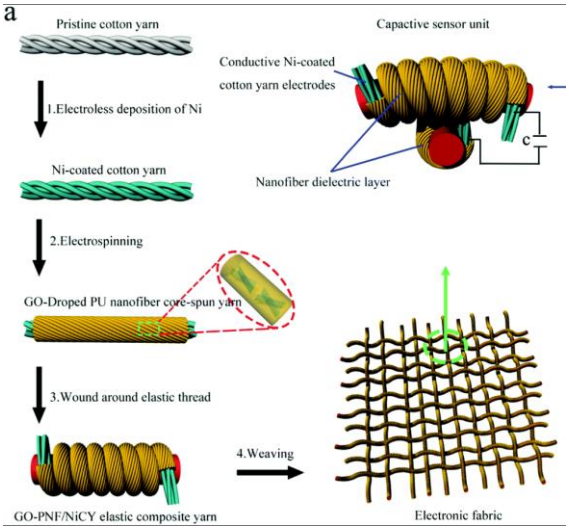

Figure 10 - A capacitive fabric used for strain and pressure sensing.
Adapted from " Stretchable capacitive fabric electronic skin woven by electrospun nanofiber coated yarns for detecting tactile and multimodal mechanical stimuli," by X. You et al., 2018, Journal of Materials Chemistry, volume 6

Each intersection was capable of detecting pressure and measurement taken across its whole length or width can be correlated with strain since applied strain will cause pressure at each intersection and also the contact area will increase. The sensor behaviour was non-linear at higher strain but had good repeatability and signal stability,

although its structure required complicated data collection equipment to simultaneously sample the capacitance across each pair of perpendicular threads.

2.2.5. Cylindrical Capacitors

To further reduce size of flat film-based capacitor, whose capacitance depend on the conductive area, and downsizing which is limited by the size needed to obtain a meaningful baseline signal amplitude that is detectable by the readout circuitry and a decent enough signal-to-noise ratio, cylindrical capacitors, with its coaxial capacitance given by:

$$C = L\frac{2\pi\epsilon\epsilon_0}{\ln\left(\frac{r_{outer}}{r_{inner}}\right)}$$

Where *L* is the length of the capacitor along its axis, ϵ is the dielectric constant of the dielectric layer, ϵ_0 is the permittivity of free space, and r_{outer} and r_{inner} is the outer and inner radius of the dielectric layer (point of contact with the electrode) respectively.

One of the earliest strain sensors that used a cylindrical shape was developed by Son et al. [45] The sensor consisted of thin walled elastomeric tubes (as the dielectric) with carbon grease painted on both sides as electrodes. The sensor was large and conformed to the inside surface of a McKibben actuator to measure the amount of actuation provided by the actuator. In this case the deformation of the sensor was driven largely by the radial expansion of the McKibben actuator. A parameter study on factors affecting the sensor performance was also completed and found that radius had much smaller effect on the baseline signal than the dielectric layer thickness, hinting that further downsizing can be achieved without compromising baseline signal amplitude.

The capacitive strain sensor developed by Frutiger et al. [23] employed a multicore-shell fiber printing method of production. Each sensor consisted of four concentric layers starting from the middle an ionically conductive liquid core, surrounded by a layer of elastomer as dielectric, further out another layer of conductive liquid, and finally encapsulated by another layer of silicone elastomer. All layers can be simultaneously printed onto a substrate to cure and later released as a free-standing fiber (Figure. 11).

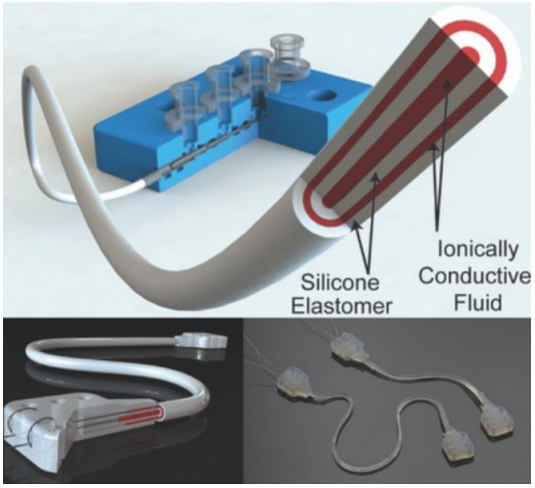

Figure 11 - A encapsulated ionic liquid capacitive sensor.
Adapted from " Capacitive Soft Strain Sensors via Multicore–Shell Fiber Printing," by A. Frutiger et al., 2015, Advanced Materials , volume 27

Frutiger's sensors showed capacitance readings linearly correlated to elongation up to 250%. The use of ionically conductive liquid as electrodes and the high permeability of the silicone encapsulation used resulted in significant water absorption over extended period, which caused inconsistencies in readings because of the resulting volume change (~30% increase as reported). The increase in volume lead to a gradual change in baseline capacitance over time. Other factors that lead to volume change include temperature and liquid leakage. At low strain, the inadequate tension would cause bending in the inner tube, causing deviations in readings.

Dip coating method has also been used to produce cylindrical capacitive sensors. Kofod et al. [47] developed multilayer coaxial fiber dielectric elastomer actuators by repeatedly and alternatingly dipping a rubber fiber in conductive and dielectric precursors. The rubber core was able to be removed to expose the inner electrode because of its inability to bond with the material selected. Kofod also demonstrated its usage as a strain sensor, but a strain of 400% applied to a 23mm sample only raised the reading from 7.6pF to 25.4pF. A low baseline and a low sensitivity was reported, and no other characterization was performed.

Further reduction in size of the cylindrical capacitive sensor without compromising performance was achieved by Wang et al. [54] Wang developed thin (160um in diameter) capacitive strain sensors by melt drawing a SEBS core filament and wrapping MWCNT aerogel sheets onto the pre-stretched (900% strain) SEBS core. The buckling

of the MWCNT aerogel sheets after pre-stretch was released lead to minimal resistance change of the electrodes when the sensor was stretched, this was beneficial to a stable performance of the sensor especially in high frequency AC circuits. The downsized sensor maintained the advantages of other capacitive sensors with good linearity, low hysteresis, and high cyclic repeatability.

Chapter 3. Prototype Sensor Fabrication and Smart Knee Brace Integration With Knee Angle Monitoring for Walking Experiment

3.1. Types of Elastomer

Elastomers are essentially polymers with the property of viscoelasticity. They are made up with long chains of mostly Carbon, Hydrogen, Nitrogen, Silicon and Oxygen atoms bonded together covalently with Carbon or Silicon often being the backbone and possesses a degree of crosslinking among neighbouring chains that plays a crucial role in the shape recovery process after elastic deformation. Elastomers are amorphous when maintained above their glass transition temperature as the polymer chains are allowed a degree of mobility that is lacking when below the glass transition temperature. The glass transition temperature is an essential indicator used to classify a plastic compound either as a thermoplastic or as a thermosetting polymer. [7]

3.1.1. Thermoplastic Elastomer

The polymer chains in a thermoplastic elastomer typically associate by Hydrogen bonding, ionic bonding or van der waals forces. The strength of the association between the chains are temperature dependant and rapidly weakens when the material is heated. Upon reaching its melting temperature, the material turns into a viscous liquid that allows rigorous reshaping and is ideal for production techniques such as injection molding and extrusion. The cooling process allows the re-association of the polymer chains and the whole heating-cooling process can theoretically be repeated although in practise some oxidation will result from each reheat attempt and gradually degrade the material's property. [7]

3.1.2. Thermoset Elastomer

Contrary to thermoplastic elastomer, the liquid-to-solid state transition that occur when a thermosetting elastomer is heated or cured is an irreversible solidification process. During the process the chains become chemically crosslinked, that is a stronger cross-linkage when compared to the intermolecular forces present in the thermoplastic

elastomer and allows better shape recovery after deformation. However, because of the irreversibility of the solidification process, the processability of the thermoset elastomer once it begins curing is very low and is used mostly in molding applications where the elastomer is formed into the desired shape over the curing period. [7]

Silicone is an example of thermosetting elastomer and is used in multiple researches in the past to produce parallel plate capacitive strain sensors. The curing process at room temperature can be initiated through a curing catalyst (typically additives containing platinum or tin).

3.2. Factors Affecting Sensor Performance

3.2.1. Mechanical Properties

Since the change in capacitance is the result of geometric change of the sensing filament, the mechanical properties of the material used in the sensor have a direct impact on sensing performance. For the purpose of monitoring movement, the ability for the sensor to geometrically track the motion closely is key for an accurate reading. To achieve this, materials need to be able to deform when a strain is applied, recover its original shape when strain is removed, and the recovery speed needs to be faster than the speed of strain removal to avoid the hysteresis effect.

A material's ability to deform and recover its shape, and the speed at which the shape recovery takes place can be determined by a combination of parameters, namely the modulus of elasticity (Young's modulus for the case of tensile deformation), elastic limit (also known as yield point), and resilience.

The relationship between these three parameters is illustrated in Figure. 12

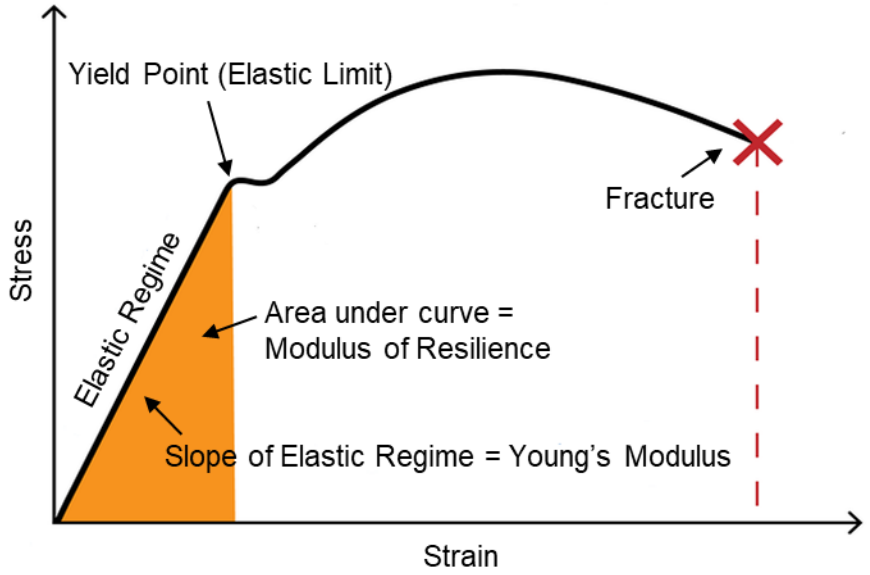

Figure 12 - Stress-strain curve of a polymer and parameters associated with its mechanical property

Young's modulus measures a material's stiffness or its resistance to elastic deformation under load. It is the slope of the elastic regime of a stress-strain curve shown above and is calculated as

$$E = \frac{\sigma}{\varepsilon}$$

Where σ is the uniaxial stress (ratio of force to the cross-sectional area) experienced by the material under the applied strain ε (ratio of change in length to the original length along the axis of deformation). Young's modulus has a unit of Pascal or Pounds per Square Inch (PSI). A material that is stiff will only deform slightly with an applied force, resulting a large increase in stress and a small strain. The steep slope for the elastic regime of a stiff material results in higher Young's modulus. Conversely a soft material has a low young's modulus and is less resistant to elastic deformation. For the soft capacitive strain sensor, it is important to select materials with a low young's modulus to allow them to be easily deformable and comfortable for wearable applications.

Yield point, or elastic limit, is the maximum stress a material can sustain before the onset of plastic (permanent) deformation. Prior to the yield point, the material is able to deform elastically and return to its original shape after the applied force is removed. After the yield point, the deformation will no longer be linear and also a percentage of the

deformation will no longer be recoverable. For the soft capacitive strain sensor, it is important for the sensor operation to stay below the elastic limit so the amount of deformation, which will be directly translated to a change in capacitance, is fully recoverable to ensure a constant baseline reading when the sensor is not strained.

Resilience measures the material's ability to absorb energy during elastic deformation and release that energy during unloading. Modulus of resilience is the area under curve during the elastic regime and measures the amount of elastic energy that can be absorbed by the material during elastic deformation. However, that energy may not be fully returned during shape recovery when the applied stress is removed and is dissipated as heat in the material. Resilience itself is commonly measured by a standard known as ASTM D2632 which is the vertical rebound method. The test involves the dropping of a metal plunger with a prescribed mass and shape (usually a sphere) on the material and measure the ratio of rebound height to the initial drop height. This ratio then represents the amount of energy returned. A material that has high resilience will return more energy during unloading which will result in a faster recovery to its original shape. For the soft capacitive strain sensor, high resilience will ensure a fast recovery of the baseline capacitance reading and minimize the effect of hysteresis in sensor operation.

For wearable applications the sensor needs to operate in a wide range of outdoor temperatures. The glass transition temperature of a material is also important in this case, the glass transition temperature is the temperature below which the polymer enters into a glassy or crystalline state where the movement of the chains become very limited, resulting in drastically different mechanical property. Choosing a material with a low enough glass transition temperature to satisfy usage in cold weather becomes a necessary consideration.

3.2.2. Dielectric Layer Thickness

The capacitance scales with the term

$$\frac{1}{\ln(\frac{r_{outer}}{r_{inner}})}$$

when the ratio of the outer and inner radius approaches one (dielectric layer is getting thinner for a given sensor dimension), this scalar approaches infinity, resulting in a large increase in capacitance baseline.

A large baseline capacitance is desirable as it reduces the effect of parasitic capacitance in the readout circuitry and the effect of ambient EMI on the reading. It also lowers the requirement for resolution for the readout circuitry [2].

3.2.3. Dielectric Constant

The dielectric constant, also known as relative permittivity, is the material's ability to become polarized with the application of an electric field. It is measured as the ratio of the material's permittivity to the permittivity of vacuum. The dielectric constant provides a linear scalar to the baseline capacitance. Any increase in the dielectric constant will result in a proportional increase in the baseline capacitance reading.

3.2.4. Equivalent Series Resistance

Equivalent series resistance of the sensor mostly comes from the electrode and lead resistance and dielectric losses. While it appears as a resistance in series with sensor capacitance and does not directly affect the capacitance reading in the sense that it does not change the theoretical baseline capacitance value of the sensor, it does alter the RC time constant of the sensor and the resonant frequency of the sensor which will have a significant impact on sensor performance in a high frequency AC circuit. This is further complicated by the presence of piezoresistivity such that the equivalent series resistance will increase with strain with a gauge factor much larger than that of the sensor capacitance change. These factors combined will affect certain system performance depending on the data collection circuitry or machinery used in the system.

3.3. Initial Design with Silicone Tube

The initial design of the capacitive strain sensor involves the coating of an already-made silicone tube, The silicone tubing was chosen for its low young's modulus and good rebound performance and is made of an unknown grade of Thermoplastic Polyurethane.

Carbon Black (Vulcan XC-72R)/silicone glue (Smooth-on Sil-Poxy) composite was first dissolved in Trichloroethylene and then coated onto the inner and outer wall of the silicone tube. While a capacitance is indeed achieved through this method, there are quite a few downsides to this design. Since the silicone tube is made to 0.6mm* 0.3mm O.DxI.D to enhance embeddability, it is very hard to deposit a thin layer of the CB/Sil-poxy layer on the inner wall of the tubing without blocking the entire bore, in which case electrical contact to the inner electrode will be hard to achieve for connecting to readout circuitries. Also, the walls of the tubing are used as the dielectric layer and is considerably thicker than the electrode coating, which is contrary to what is desired (ratio of outer and inner radius close to 1). With the silicone dielectric used in the sample having a dielectric constant of 1.3, and a thick dielectric layer the base line reading is 9pF, as an unshielded capacitor, stray capacitance from the readout circuit (~4pF) and ambient EMI resulted in a low signal-to-noise ratio.

3.4. Material Choice for Prototype Sensor

For the purpose of a wearable strain sensor. The materials must have high elasticity and resilience. Ideally, materials with close to rubber elasticity (hyper-elasticity as seen in the case of natural rubber) is preferred as the backbone of the sensor to provide the bulk of its mechanical property and the elastic behaviour in this case will allow the sensor to fully recover its baseline reading and produce linear repeatable readings within the wider elastic region. This hyper-elasticity is represented as an extended linear region before the material hit the yield point at a certain strain%. The processability of the material is also an important factor as it affects the achievable shape and scalability of the production procedure. RTV Silicone elastomer was first ruled out due to the difficulties in miniature molding it into a thin and uniform filament. After comparing available thermoplastic and thermoset elastomers in terms of their processability and availability, polyether-block-amides (Pebax 3533, Arkema) [73] and polyester-ether co-polymer (Hytrel 3078, DuPont) [72] are chosen for their high resilience and low modulus for certain grades. Both materials are easy to process and designed for extrusion and injection molding. These high-resilience materials also have a low glass transition temperature of below -40℃ which warrants their elastomeric properties at a wide range of temperature, and thus very suitable for wearable applications in various temperature conditions.

3.5. Sensor Fabrication

While the thermoplastic material was chosen to suit melt extrusion and injection molding purposes, the lack of a micro-coextrusion system capable of extruding multilayer micro-tubing was not available at the time of the completion of this thesis. Instead, a solvent based approach was used to achieve the required layers.

Hytrel 3078 was first extruded at 190℃ into a 400um diameter filament to serve as the core of the sensing filament. This bare filament was the backbone of the entire sensor structure and provides the bulk of its mechanical properties that is free from any changes caused by additives. 5% (w/v) Hytrel 3078 and 5% (w/v) Carbon Black (XC-72) in dichloromethane solution is prepared as the electrode coating solution. 5% (w/v) poly(Styrene-b-Ethylene-co-Butylene-b-Styrene) (SEBS) was dissolved in cyclohexane as the dielectric coating solution. There are several reasons for using SEBS as the dielectric layer material instead of using just Hytrel-Dichloromethane solution. One is that SEBS has decent mechanical property that can cover the elastic region of Hytrel although it is not as resilient as Hytrel. Another is that the cyclohexane solution used to dissolve SEBS is a non-solvent for Hytrel, and this prevents the coated Hytrel core to redissolve or swell when submerged into the coating solution. Although the Hytrel material has a relative permittivity of 4.9+ which more than doubles that of SEBS, the porosity of the layers obtained from the current method allows outer electrode solution (Hytrel-CB composite in dichloromethane) to permeate through resulting in insufficient insulation as can be seen in Figure.15a.

Unlike the hollowed tube method, access to the inner electrode needs to be achieved through a special coating procedure described below in Figure. 13:

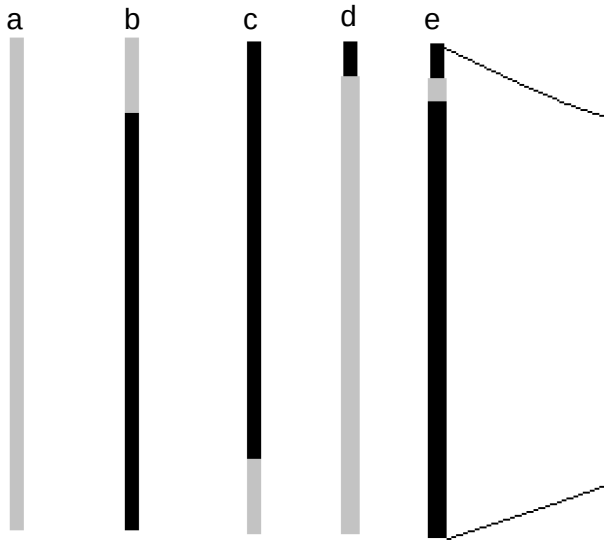

Figure 13 -Fabrication procedure for the dip coated sensor

a) Extruded Hytrel 3078 core

b) Coat with CB-Hytrel composite while leaving a small region at the end in preparation for the next steps, vacuum oven to remove excess solvent. This layer will serve as the inner electrode.

c) Reverse the filament, the uncoated portion will ensure an electric insulation between the electrodes. If the filament is fully coated in b) the electrodes often short at the ends.

d) Coat with SEBS solution, vacuum oven to remove excess solvent in between, leave the top region out as electrical contact for the inner electrode, repeat multiple times to achieve proper insulation.

e) Coat with CB-Hytrel composite up to slightly lower than the dielectric layer as the outer electrode, vacuum oven to remove excess solvent, electrical connection to the inner and outer electrode can be achieved at the ends (with electrical connection to the outer electrode achievable anywhere along the outer coating).

A syringe pump placed vertically on a laboratory jack was used as a dip coater (Figure.14) . The Hytrel filament is secured to the syringe pump at one end and weighted down at the other end to ensure a straight filament for dip coating.

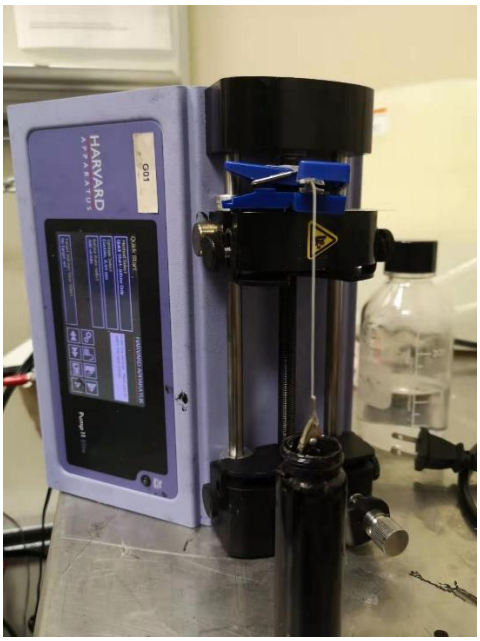

Figure 14 - Dip coating apparatus: Vertically placed synringe pump, clamped tweezer on linear stage, and vial for dip coating solution

It was found the maximum speed for the pump is approximately 2mm/s, which is considerably low compared to a typical dip coater (maximum draw speed from 20mm/s to 150mm/s available).

The low dip and draw speed create a few challenges. The low draw speed resulted in very thin layers that is 5-10um thick despite increasing the SEBS-cyclohexane solution to 10% wt-vol concentration. The porosity combined with the thin thickness of the dielectric layers resulted in inadequate insulation between the inner and outer electrodes since the outer electrode coating can permeate the insulating SEBS layer if it is too thin (dichloromethane can dissolve SEBS). and multiple layers of the dielectric polymeric solution must be applied before a capacitance can be established. The low dip speed however complicates this process since dipping additional layer with a slow speed resulted in some degree of re-dissolving of the already-applied SEBS layers. This was observed as the increasing roughness of the coated surface as more and more layers are added on.

Figure.15b shows the re-dissolving of the SEBS layers with a slow dipping and drawing speed after applying multiple layers evident in the peeling and cracking in the applied layers

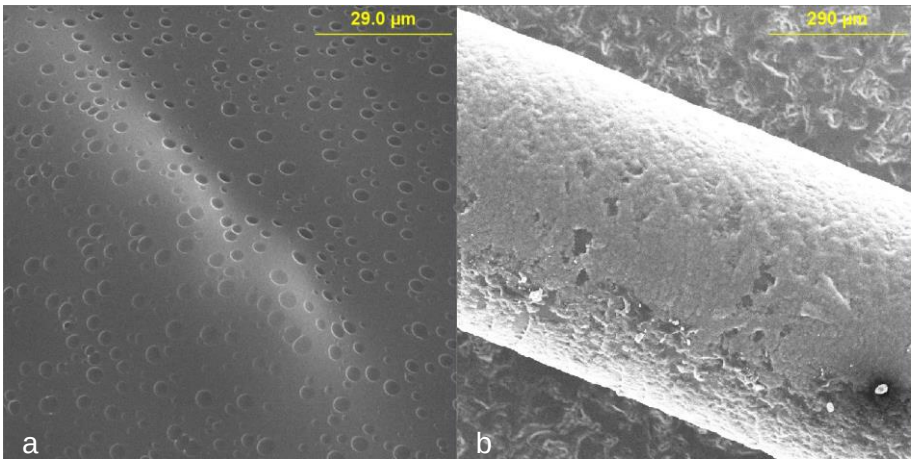

Figure 15 - a) Dielectric layer coated with Hytrel 3078 in Dichloromethane solution showing porous structure. b) SEBS dielectric peeling and cracking after long exposure in SEBS-Cyclohexane solution

To address this problem, a laboratory jack was used for quickly lowering the filament into the dielectric solution manually and the syringe pump was only responsible for the drawing process so that average surface exposure to solvent was halved, however the manual lowering of the lab jack resulted in different dipping depth and thus a uneven shape of the sensor which was later evident in the non-linear behaviour of the sensor that was different from a predicted linear model.

Sensors produced through this method are 4 to 5 cm long and have diameter of 500um. The base capacitance reading ranges from 60 to 120 pF.

The produced sensor was demonstrated to have repeatable readings during loading-unloading cycles as illustrated in Figure.16. A 37.4mm sample was subjected to 10 cycles of 20% strain on a linear stage and data was collected with a 555-timer astable multivibrator capacitance readout circuit described in the following chapter.

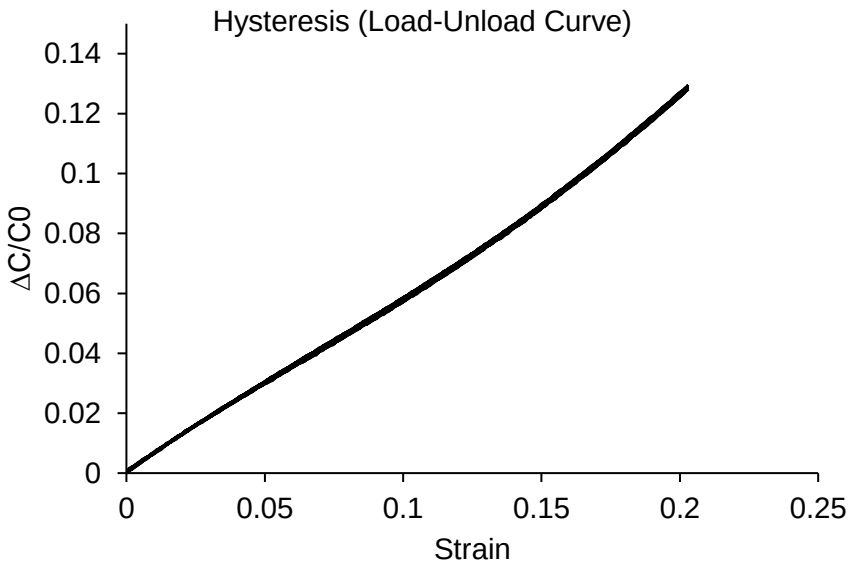

Figure 16 - Hysteresis curve for prototype sensor showing non-linear behavior

The 20% strain stays within material elastic region and the sensor observed negligible hysteresis with overlapping load and unload performance. The capacitance reading of the sensor is increased by approximately 13% in response to a 20% applied strain and the gauge factor is thus calculated to be 0.65, which agrees with previous researches suggesting the gauge factor will be lesser than or equal to one. Another simple test was performed where the sensor was held at a random strain for 10min and only a 0.05% variation in the sensor reading is observed. This sets ground for a knee brace prototype that can produce repeatable and stable readings when subjected to extension caused by knee flexion. The performance of a prototype knee brace with the prototype capacitive sensing filament embedded will be discussed in the following sections.

3.6. Knee Brace Prototype and Knee Angle Monitoring for Walking Test

3.6.1. Preliminary Bending Stage Test

To test the capacitive strain sensing filament's ability to detect bending and to explore the relationship between angle and sensor extension and capacitive reading. A preliminary test was done on a bending stage fabricated in the MENRVA lab. The bending stage consists of two wooden blocks connected with a rotational joint with a

single degree of freedom. An electronic protractor is attached on the side of the bending stage to measure the current angle. The whole setup is shown in Figure.17

Figure 17 - Bending stage test setup

The system was designed to mimic a one-degree-of-freedom joint such as a knee or an elbow joint where the sensor's extension will be most pronounced when placed perpendicular to the rotational axis of the joint, Sensor was secured to Velcro pads on the two ends through sewing and electric taping and electrical connection is achieved through copper wire and electric tape, the Velcro pads were then secured on Velcro pieces glued on the wooden blocks of the bending stage. Sensor data was collected using the 555-timer astable multivibrator capacitance meter circuit and logged by a Python script into a csv file. The bending stage was kept at angles from 180 degrees to 90 degrees in decrement of 10 degrees and hold at each stage for a period of time to allow averaging of capacitance reading and the averaged capacitance reading was manually logged along with the protractor angle. The result is plotted in Figure.18

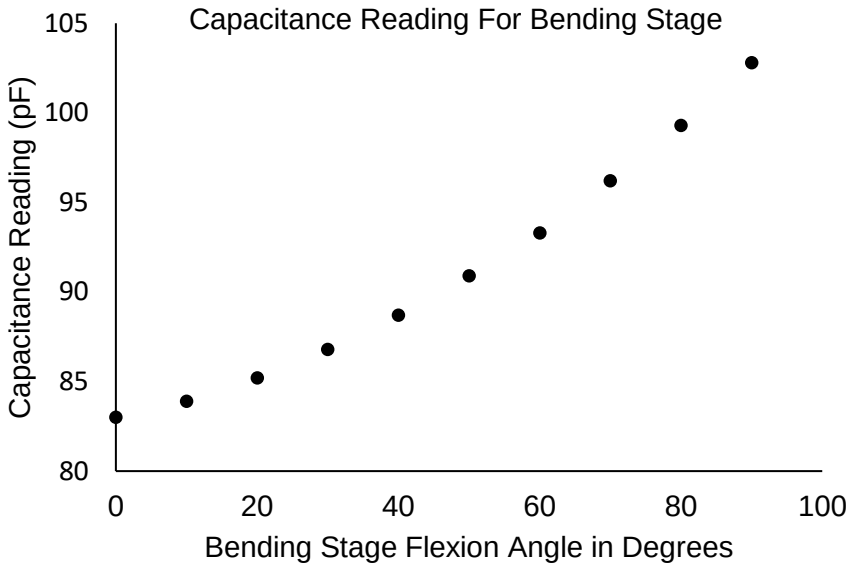

Figure 18 - Bending stage test capacitance reading for different stage flexion angles

A quadratic relationship between the angle and the capacitance reading was observed. As the bending angle increases the capacitance increases at a faster rate and this was attributed to the slightly elevated joint of the bending stage that provided larger tension in the sensor at larger flexion (similar to the presence of patella of the knee). A polynomial function was fitted to the data to predict angle with given capacitance readings and the predictions were found to deviate from the true angle seen on the protractor by less than 1 degree.

3.6.2. Knee Anatomy and Sensor Placement

The knee is one of the largest joints on the human body and is made up of femur (thigh bone), tibia (shin bone), fibula (smaller bone beside tibia), and patella (kneecap). Ligaments join the bones together to prevent sliding and provide stability to the joint and movements are achieved with tendons connecting the bones to leg muscles (Figure. 19).

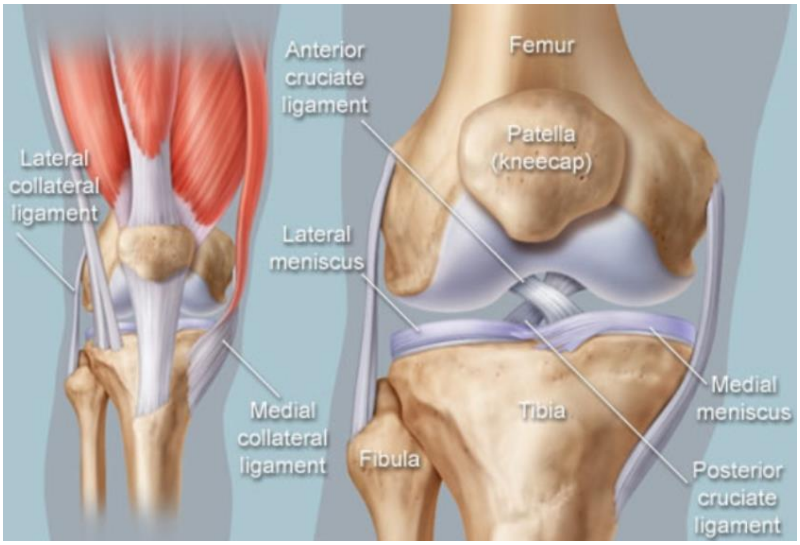

Figure 19 - Anatomy of human knee.
Adapted from " Knee (Human Anatomy): Images, Function, Ligaments, Muscles," by M. Hoffman, WebMD. Retrieved November 10th, 2019, from https://www.webmd.com/pain-management/knee-pain/picture-of-the-knee

The main movement of the knee is flexion and extension, during which the knee acts as a hinge joint and allow gliding of the articular surfaces of the femur over the tibia surface. This allows movement along one plane. The range of motion is typically 0℃ for extension to 140℃ for flexion.

3.6.3. Sensor Embedding: Knee Brace for In Situ Knee Joint Angle Monitoring

The capacitive strain sensing filament provides a one-dimensional data based on strain. Ignoring the effect of parasitic capacitance and ambient electromagnetic interference and errors caused by external circuitries, the performance of the sensor itself largely depend on the extent to which the monitored parameter can be translated to a strain that is to be observed by the sensor. For the purpose of knee angle motion tracking, the extension in the skin as the direct result of knee flexion and extension can serve as a base to utilize the capacitive strain sensing filament. Choi et al. [13] studied the skin deformation during lower extremity motions with 3D body scans with a dense grid of markers placed over lower extremity skin. It was found that the skin above and below the knee cap all experienced noticeable deformation during lower body motion and both horizontal and longitudinal extension of the skin are present with horizontal extension caused by muscle activation, and longitudinal extension caused by bone movement. A

knee brace with sensor embedded vertically above the patella is proposed based on this information. The amount of extension experienced by the skin to be transferred to the surrounding textile not only depend on the magnitude of the skin extension, it also depends on the friction between the textile and skin. With friction being calculated as

$$f = \mu N$$

Where μ is the coefficient of friction between the skin and fabric, N is the normal force. The coefficient of friction between the skin and surrounding fabrics are affected by factors such as skin texture, skin moisture level and fabric type [52] with an increase in skin moisture level showing significant increase in coefficient of friction. While [52] studied used Vaseline to moisten the skin, this practise is unusual in a daily setting, and hence it was decided to add silicone lining tape linings along the insides of the knee brace to mimic the effect of moist skin and increase the friction. The normal force was maximized by using a small sized knee brace that provided skin-tight support to the knee.

The sensor can be sewn thanks to its small diameter with a flat stitch pattern to allow stretching on fabrics as shown in Figure.21

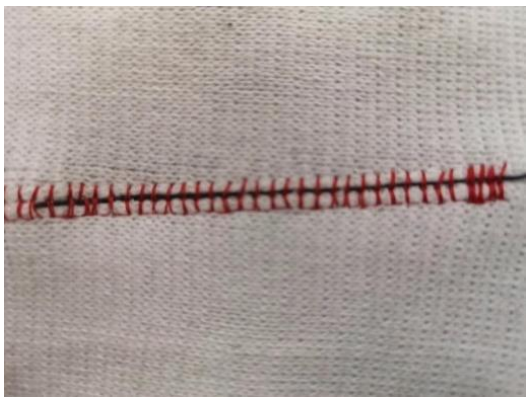

Figure 20 - Sensor embedding by sewing technique to allow stretching

Balancing the thread tension can be a challenge as too much thread tension creates noise in the reading as radial compression on the sensor from multiple points alter the capacitance. The tight stitches prevent an even distribution of stress along the sensor, but too little tension allows the sensor to slide along the “tunnel” formed by the thread and the fabric. It was found that the sensor performed best when no significant compressional force was present on the sensing region (i.e., no tight stitches). The

sensor was weaved into a knitted knee brace long the longitudinal direction above the patella and secured on both ends with a metal snap button which also serves as the electrical contact to the sensor electrode. The coating methodology employed allow the sensor to be easily connected similar to other soft strain sensors on the two ends. The embedded sensor is shown in Figure.22

Figure 21 - Sensor embedding through weaving in knee brace with metal snap buttons and conductive thread

Conductive thread was soldered on the metal snap button to establish connection to the external readout circuitry. The hole on the patella provides a position reference for putting on the knee brace and also an anchor point, this combined with the silicone tapings on the inside and the tightness of the knee brace ensures minimal sliding and the maximum transfer of skin extension to the fabric.

To test the knee brace's ability to track knee angles, a video-based motion capture system (Vicon, Oxford, UK) was employed as ground truth for the knee angle, three markers, MK1, MK2, and MK2 were placed on the side of the femur, the patella and the tibia respectively (Figure. 23) and a knee angle was calculated by dot product of the vectors formed between MK1-MK2 and MK2-MK3

Figure 22 - Reflective marker placement for motion tracking system

A simple series of knee flexion and extension was performed, and sensor data was collected using the 555 timer circuit to read capacitance with an integration window of 1/60s to match the sampling rate of the motion capture system. The proximity of the sensor to skin, the relatively shorter integration window and the unshielded conductive thread connecting sensor to the readout circuitry resulted in noticeably increased noise. After applying a low pass filter on the data, the reference knee angle and sensor reading was plotted in Figure.24 top.

The knee brace reading increases as the knee angle decreases (flexion) and decreases as the knee angle increases (extension) as expected and captured the amplitude characteristics of each flexion-extension cycle. A second-degree polynomial was fitted to the result in Figure.24 bottom using MatLab polyfit function to obtain a best fit with a least-squares approach.

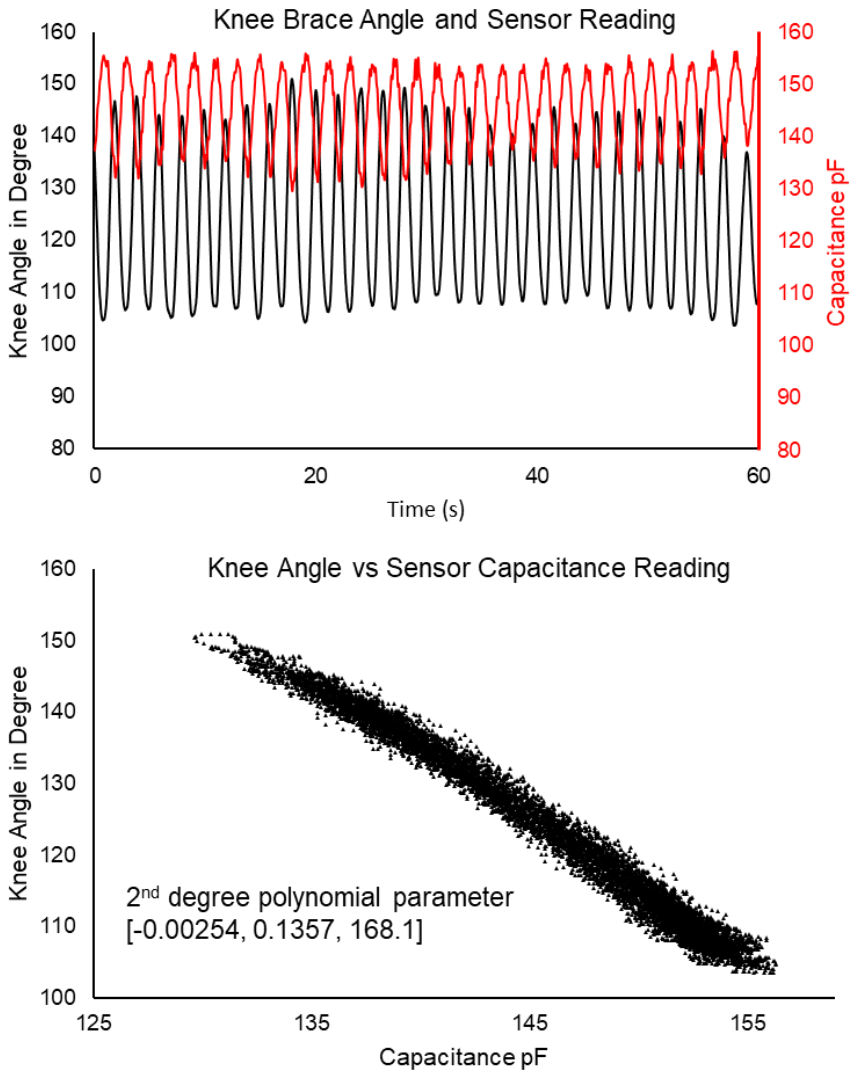

Figure 23 - Top: Sensor reading for simple knee flexion and extension. Bottom: Sensor reading versus Knee angle data points used for polynomial fitting

The polynomial was used to predict a 20-second section of the raw data that was not used for the curve fitting and the result is shown in Figure 25 where raw sensor output was used as the input to the polynomial, and the predicted knee angle is obtained as output. :

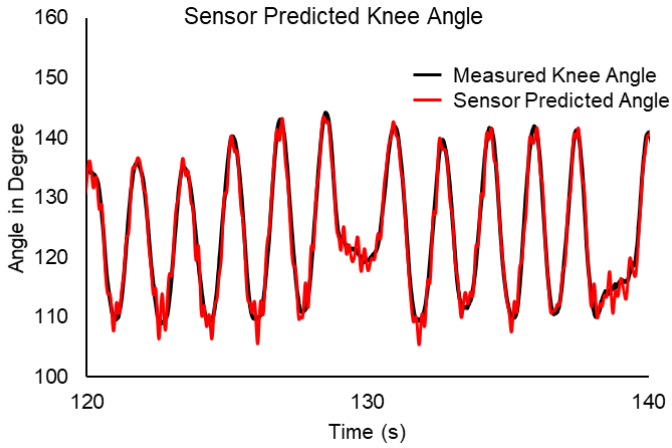

Figure 24 - Sensor predicted knee angle for simple flexion and extension

The Root Mean Square Error was calculated to be 1.6 degrees, which was about 1% error of the baseline of approximately 160 degrees when relaxed. A similar knee flexion-extension test was performed by Totaro et al. [49] with a similar range of motion and with flat parallel plate capacitive sensors embedded on a knee brace, three sensors are embedded alongside of each other in order to exploit sensor redundancy and achieve better correlation. Totaro et al. reported a root mean square error for their knee flexion and extension test of less than 4 degrees with a first-degree polynomial (their sensor had better linearity than the current prototype). Frutiger et al. weaved their multicore-shell fiber sensor with ionic liquid into a lower body tights, although they did not use motion tracking to provide a reference angle for error calculation. Their sensor performance can be observed in a video [23.S4] which shows large error in capacitance during knee extension that was not present in this study although their sensor performed better in resistive mode as shown in Figure.26.

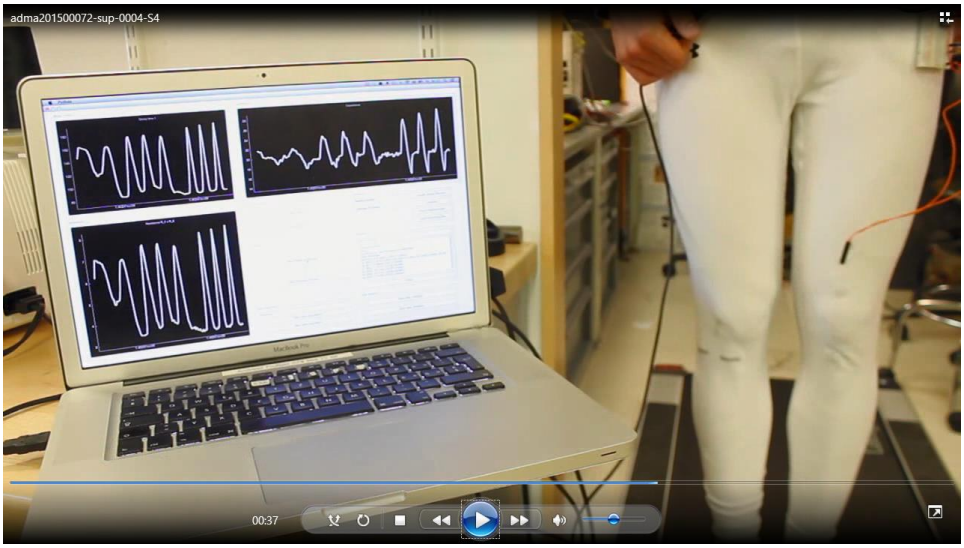

Figure 25 - Video screen capture showing ionic liquid capacitive strain sensor showing large error when knee is fully extended Top right shows the capacitance reading, bottom left shows the resistive reading.
Adapted from " Capacitive Soft Strain Sensors via Multicore–Shell Fiber Printing," by A. Frutiger et al., 2015, Advanced Materials , volume 27

3.6.4. Calibration Method and Real-time Knee Angle Tracking for Walking

In a realistic scenario, a video-motion capture system will not be available for calibration purposes and a large angle versus capacitance dataset used for machine learning/regression purposes will not be viable for the calibration process. The robustness of the sensor in terms of its deterministic signal allows a simple calibration method that can easily be performed by patients in a home setting.

Calibration Protocol:

- Step 1. Put on knee brace while sitting, fully extend leg, align kneecap with the hole on knee brace, pull the upper rim of the knee brace so the sensor is slightly pre-strained. Log the baseline reading.
- Step 2. With a protractor, measure knee angle and hold the angle at 160, 150, 140, 130, 120, 110, 100, 90 degrees for 10 seconds each, average the sensor reading to compensate for noise.
- Step 3. Fit polynomial on the Angle-Capacitance data obtained in Step 2
- Step 4. Sensor can now output calculated angle based on the polynomial and sensor reading.

Prior to the walking test, the above protocol was performed to obtain the polynomial model for the sensor. Protractor was aligned with the reflective markers used by the motion capture system to measure angle (Figure.27) and capacitance reading was averaged over each angle hold period.

Figure 26 - Calibration process, protractor measuring marker (knee) angle

The polynomial model for the test is shown in Figure.28:

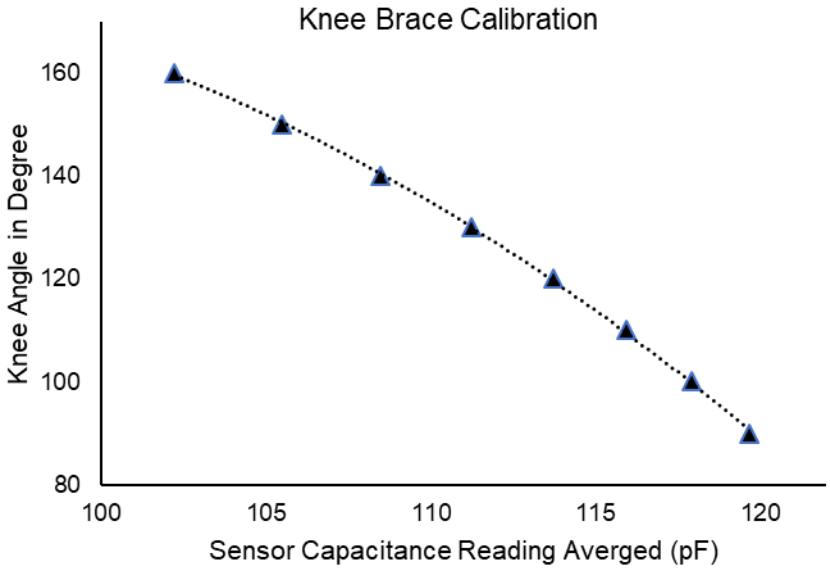

Figure 27 - Calibration measured angle versus knee brace sensor reading and fitted polynomial

After calibration a walking test was performed on a treadmill (Bertec Corporation, Columbus, OH, USA) at a speed of 8km/hr and knee angle data was captured by the motion capture camera and the sensor reading was captured with the 555 Astable Multivibrator circuit, with tension maintained in the conductive thread that connects to the readout circuitry so it was not hanging near the leg to be affected by EMI in an attempt to lower noise. Data is collected by the 555 Timer Astable Multivibrator Circuit with an integration window of 0.05 second for better noise performance and resulting reading was interpolated to match motion tracking sampling frequency. A comparison of the predicted angle and the reference angle for a 10-second time window is plotted in Figure.29a

It is worth noting that during both the simple flexion-extension test and the walking test, the sensor reading increases at a slower rate for larger flexion contrary to the bending stage. This can be explained by the stretching limit of the knee brace fabric. At larger flexions nearing the fabric's extension limit (which measures to be approximately 35%), there was a larger pull on the surrounding skin to compensate for the inadequate force needed to further deform the fabric. The sensor experienced minor plastic deformation after the test and the baseline was slightly increased (Figure.29b and c). No noticeable slide of either the sensor or the knee brace itself because of the robust fixtures such as metal snap buttons and a combination of tight size and silicone linings. The root mean square error between the prediction and the actual angle was 1.79 degrees, approximately 1.1% of the relaxed angle of 170 degrees. The error was still considerably lower than previously reported of 4 degrees in spite of the more vigorous movements involved during walking at relatively fast speed at 8km/hr. Minor plastic deformation was present in the knee brace after the walking test and it can explain the overestimation of flexion especially after the walking test is done. The sensor performed better when strained than when fully relaxed and hence pre-strain is always needed for ideal sensor performance.

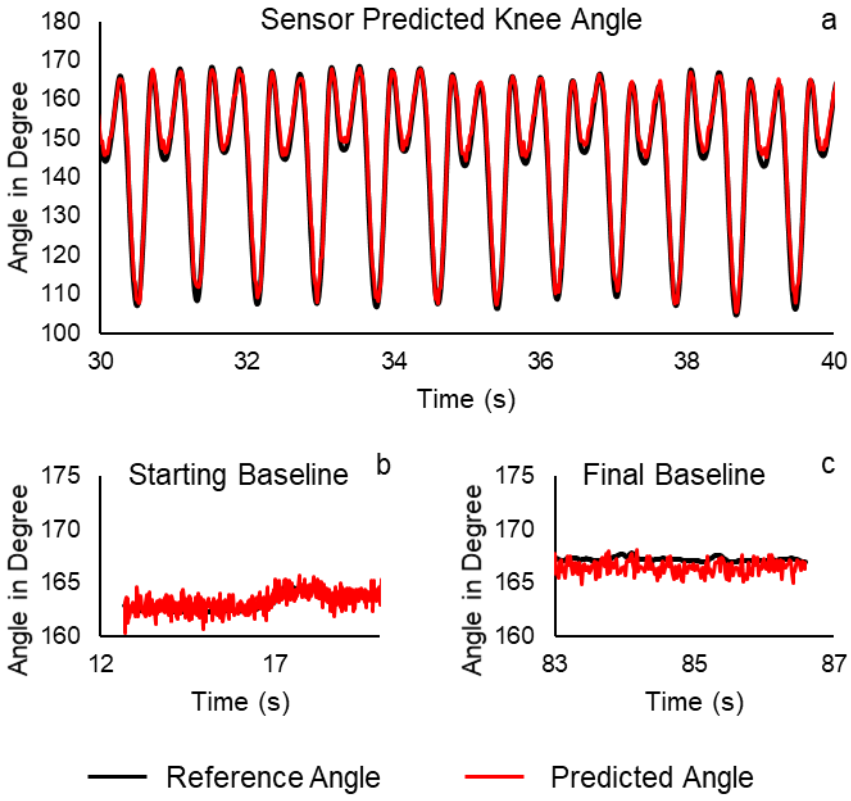

Figure 28 - Walking Test a: Comparison between sensor predicted angle and motion capture reference angle; b: Predicted baseline before walking test, c: Predicted bottom line after the walking test

3.7. Chapter Conclusion

This chapter addresses objective 3 of the thesis. The smart knee brace with the prototype sensor embedded achieved a 99% accuracy rate for tracking knee angle during an 8km/hr walking test. The result was better than the 96% accuracy rate reported in [49] with an array of 3 sensors. This can be attributed to the modification of the knee brace to ensure maximum friction between the knee brace and skin. The sensor used for the knee brace as a baseline reading of 110 and a non-linear behavior, although these characteristics did not hinder the performance of the angle prediction since repeatability was more important for tracking angles, these parameters can definitely be improved to serve a wider range of applications. Improvement of the sensor will be covered in Chapter V of this thesis.

Chapter 4. Capacitance Data Collection Circuitry

A successful sensor system needs a reliable data collection method. There are many methods that can measure capacitance. Different ways to achieve a capacitance measurement with a particular focus on reducing electronics size for embeddability are explored in this chapter.

4.1. DC Direct Charge Method

This method is the most straight forward and involves the least number of components to complete. The sensor was connected to a microcontroller (Arduino Nano) with a known resistance in series and the microcontroller supplied a 5V voltage to charge the sensor through the known resistance R. In this RC circuit the time it took to charge the sensor to 63.2% of the supply voltage was

$$\tau = RC_{sensor}$$

The microcontroller measured the time it took for the voltage across the sensor to reach 63.2% of supply voltage (τ) and then sensor capacitance is calculated as:

$$C_{sensor} = \frac{\tau}{R}$$

Here the equivalent series resistance becomes a considerable source of error as the piezoresistive material used in the sensor creates a resistance R_{ESR} that will change based on the strain applied and has hysteresis and drift characteristics similar to that of a resistive strain sensor. The sensor reading then becomes:

$$C_{sensor} = \frac{\tau}{R + R_{ESR}}$$

Since the equivalent series resistance was unknown, this introduced noise and drift in the reading and was not suitable for measuring capacitive sensors with a varying equivalent series resistance. The source of the ESR was mainly from the sensor lead and the resistance of the sensor electrode material. A typical response of the sensor's equivalent series resistance is shown in Figure.30

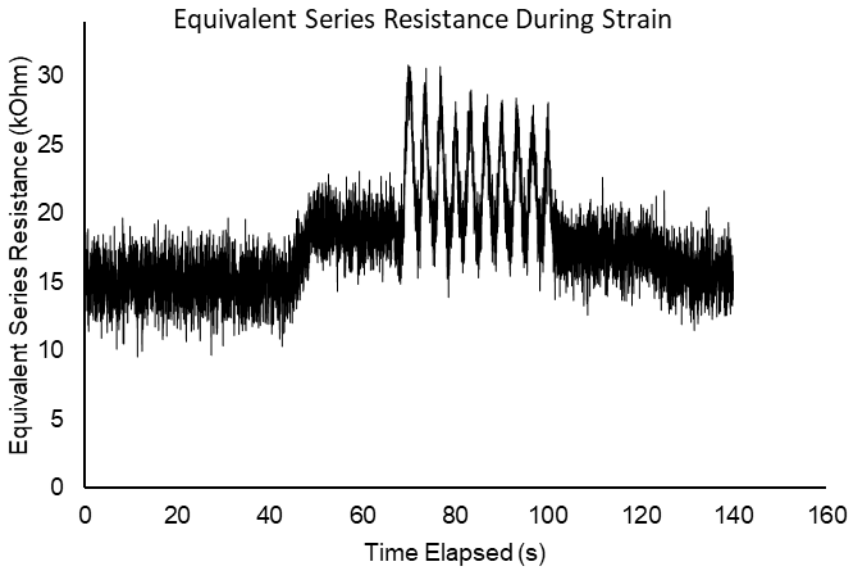

Figure 29 - Typical equivalent series resistance of the sensor prototype during a triangular strain

The sensor was strained to 5% (initial increase) and then subjected to 10 cycles of triangular wave with a strain of 10% in a tensile tester (Instron E10000) and equivalent series resistance is measured by a precision impedance analyzer at 10kHz (Keysight E4990A).

While choosing a large R theoretically lowers the effect of the change in equivalent series resistance, which typically ranges from 10kOhm up to 150kOhm, an R value of 1.3MegOhm was chosen and sensor reading under a triangular strain pattern was recorded and filtered with a low pass filter and data collected is shown in Figure 31.

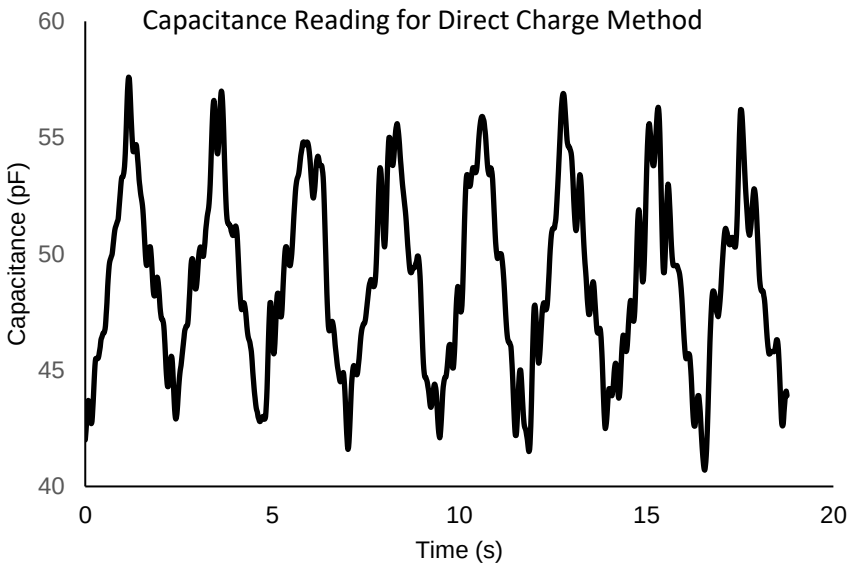

Figure 30 - Capacitance data collected by the DC direct charge method

The large resistor used to charge the capacitor resulted in very small charging current (approximately 3uA), this amplified the effect of induced current in the circuit because of proximity and ambient noise. The effect of thermo noise common in large resistors may also contribute to the noise in the capacitance reading in the form of a parasitic AC current superimposed on the DC current going into the capacitor.

4.2. LC Tank Circuit Resonant Frequency Modulation

A common way to measure capacitance is to drive a frequency that can be modulated by the capacitance under test (another example discussed in section 4). One very popular example of these frequency circuits is an inductor-capacitor resonant circuit (tank circuit) as shown in Figure.32

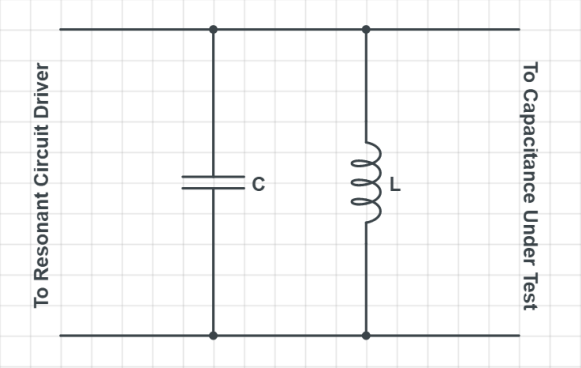

Figure 31 - A parallel LC resonant circuit

The LC tank circuit will be driven by an external resonant circuit driver to ensure a continuous oscillation (compensate for any energy dissipation in the circuit) and the resonant frequency is given by:

$$f_0 = \frac{1}{2\pi\sqrt{LC}}$$

Upon connecting an unknown capacitance C_{test} to be tested, the new resonant frequency will change to

$$f_{new} = \frac{1}{2\pi\sqrt{L(C + C_{test})}}$$

The frequency can then be fed to a counter to be measured. The capacitance under test can be calculated as the frequency, the inductance and the capacitance of the original tank circuit are all known.

An example that utilizes this technology is Texas Instrument's FDC 2x1x capacitance-to-digital converter series, where the frequency generated by the resonant circuit (original LC tank + capacitance under test) is measured through a reference frequency generated by an internal clock on board and this information is used to produce a capacitance reading. When the capacitive strain sensor is attached to the FDC circuit, the effective circuit becomes: Figure 33

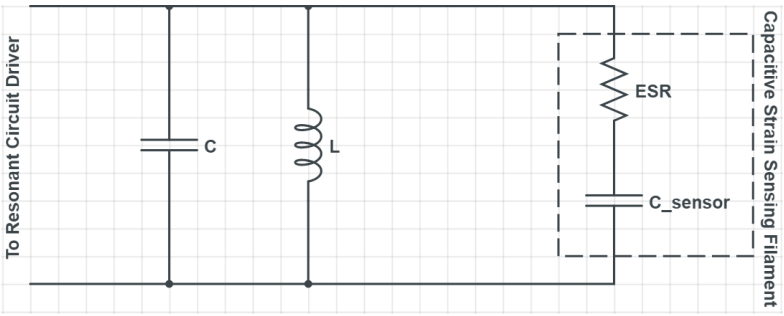

Figure 32 - A parallel LC resonant circuit with sensor attached

Since the equivalent series resistance is very large compared to traditional capacitors (kiloOhm range) and is changing with a larger gauge factor because of piezoresistivity than the change in the capacitance of the sensor (C_sensor), the effect of the ESR on the resonant circuit was explored through a circuit simulation where a parameter sweep was done on the circuit with C = 10pF, L = 100nH. Assuming minimal ESR in the circuit at 3 Ohm, stepping C_sensor from 80pF to 160pF at 20pF steps which was the typical range of reading of the current samples. The resonance frequency happening at maximum gain and 0 phase is shown in Figure.34

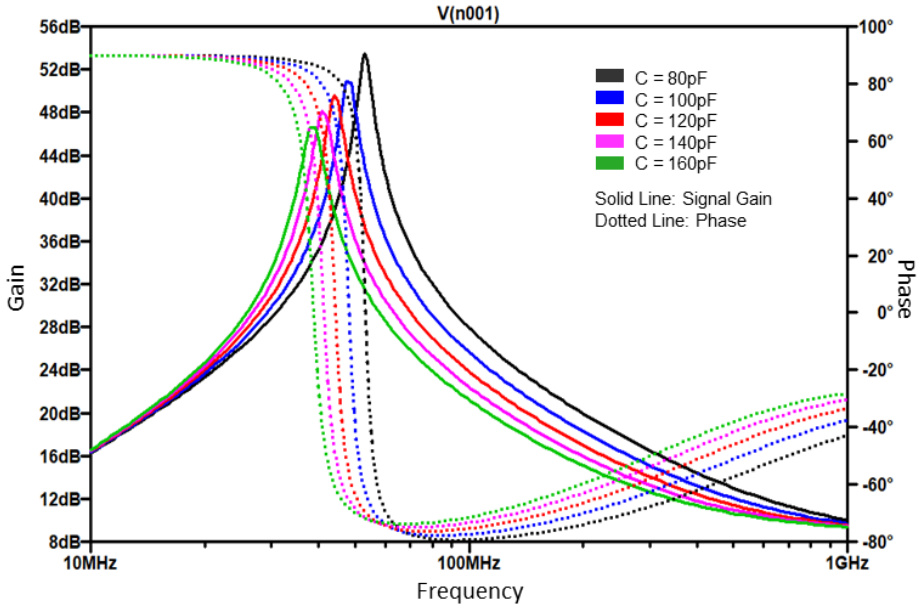

Figure 33 - Changes in resonant frequency caused by increasing capacitance assuming minimal ESR. From black is with small capacitance to Green is with large capacitance

A clear change in the resonance frequency can be observed. An increase in sensor capacitance would decrease the resonance frequency and the FDC chip will function as

expected in this case. But when there is a large ESR present in the circuit, in this case a typical 20kOhm ESR is simulated and the sensor capacitor is still stepped from 100pF to 250pF, the resonance frequency is shown in Figure. 35

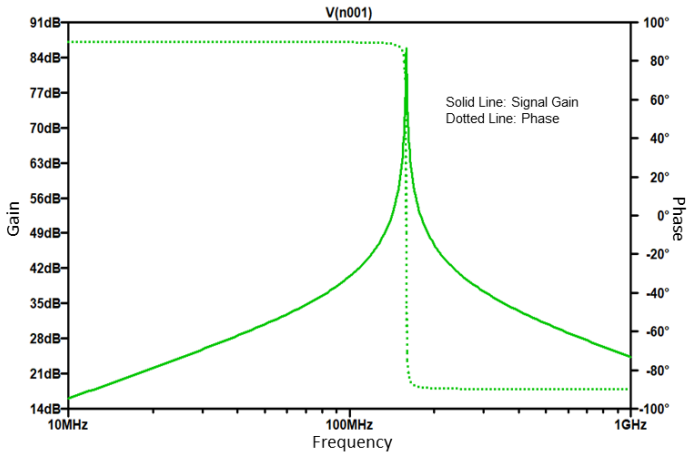

Figure 34 - Effect of high ESR on the resonance frequency, changing capacitance no longer change the frequency

At this point the change in capacitance no longer affects the resonance (as can be seen by over lapping gain and phase curve). An experiment was done on the FDC chip and the chip indeed was not able to read the capacitance change of the current sensor.

Upon further exploration, changing the on chip LC tank and lowering the original resonant frequency to C = 1nF, L = 1mH, and a parameter sweep was performed for both the ESR and sensor capacitance (both increasing at different rate for each step). The combination of the increase in ESR and capacitance resulted in an increase in resonance frequency that will be perceived as a decrease in capacitance by the FDC2212(Figure.36)

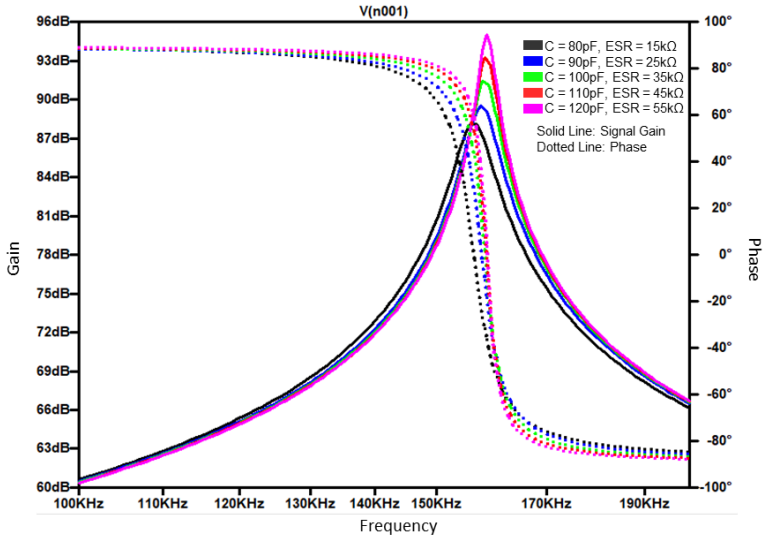

Figure 35 - Changes in resonance frequency while increasing sensor capacitance and ESR simultaneously

To verify the above simulated result, an experiment was performed with the FDC2212EVM with the factory LC tank switched to a 1nF capacitor and a 1mH inductor. The sensor used has a baseline capacitance of 89pF and a baseline ESR of 19kOhm. The step-and-hold strain applied was 10% with the sensor capacitance increasing to approximately 95pF and the ESR increasing to 43kOhm. The raw resonance frequency output was plotted in Figure 37a and the calculated capacitance was plotted in Figure 37b

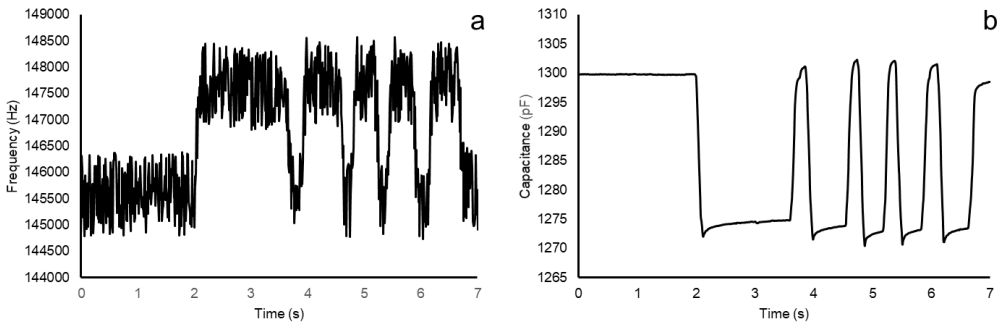

Figure 36 - Sensor Capacitance captured by FDC2212EVM showing reverse behaviour and resistive hysteresis and creep

The combined increase in both sensor capacitance and sensor ESR resulted in a large increase in resonance frequency (Figure37a) as predicted by the simulation in Figure 36. This increase in resonance frequency resulted in a decrease in capacitance observed by FDC2212EVM (Figure37b). During static load, the ESR experiences a stress relaxation

similar to that of a resistive strain sensor and the ESR gradually decreases, resulting in a drift in the calculated capacitance value that is increasing under static load in Figure37b. The calculated capacitance value is in the nF range since the FDC2214EVM combined the capacitance in the LC tank (1000pF), the sensor capacitance (89pF), the perceived capacitance from the ESR (resulting from a change in resonance frequency that is approximately equivalent to a 200pF capacitor), and all on board parasitic capacitance.

In conclusion the readings obtained by the LC tank oscillation method included the hysteresis and drift that is characteristic in a resistive sensing application, and shows a reverse behaviour for capacitance readings, and no longer has the advantage of a capacitive sensing mechanism.

4.3. Charge Balancing Circuit

The idea of using a charge balancing circuit to measure capacitance can be implemented by the working principles of Sigma-Delta(Σ−Δ) Analog-to-Digital Converters as shown in Figure.38

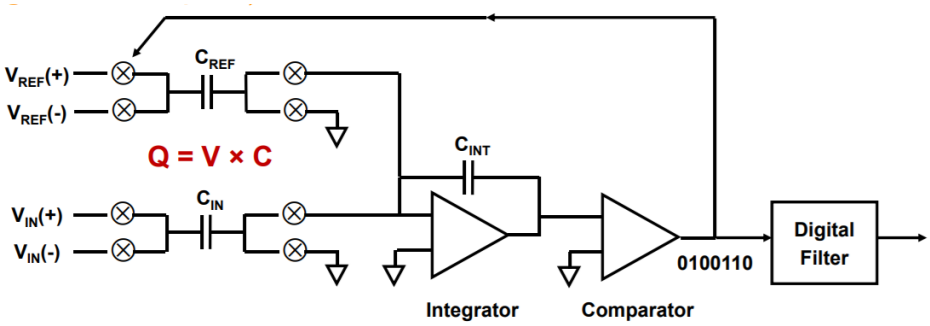

Figure 37 - Sigma Delta Analog to Digital Converters

Where both C_{IN} and C_{REF} transfer charges to C_{INT}, the integrator acts to sum up charge from C_{IN} and C_{REF} (polarity of the charge transfer determined by comparator output) and the feedback loop acts to keep integrator output at zero average over time, hence guaranteeing average C_{REF} charge equalling C_{IN} charge and the output of the comparator is the ratio of V_{REF} to V_{IN}. In this ADC set up, C_{IN} is constant and V_{IN} is the interested variable. Reversing this constant and variable relationship allows us to digitize the ratio of C_{REF} to C_{IN} as shown below in Figure.39:

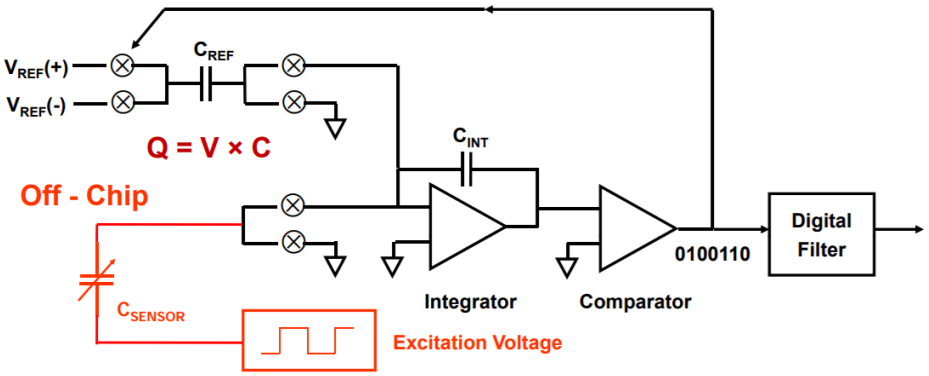

Figure 38 - Sigma-Delta Analog-to-Digital Converter in capacitance measurement (charge balancing) mode

Where the excitation voltage V_{EXC} is kept constant and the capacitance of the sensor is varying. With V_{EXC}, V_{REF} and C_{REF} known and constant, the digitized output of the comparator will be the ratio of C_{REF} to C_{IN}.

One IC utilizing this technology is Analog Devices AD7745/AD7746 Capacitance to Digital Converter [74]. The low input range (up to 17pF fixed capacitance with $\pm$4pF dynamic range) can be improved through a range extension circuit (Figure. 40) that decrease the excitation voltage by a factor to ensure the charges transferred by the sensor remains within the input range of the chip:

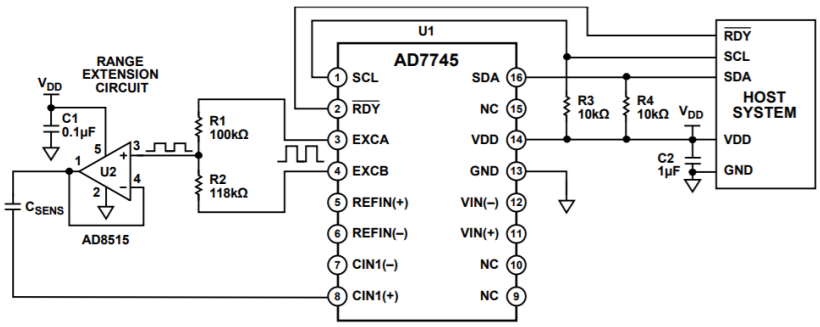

Figure 39 - AD7745 range extension circuit
Adapted from "Extending the Capacitive Input Range of the AD7745/AD7746 Capacitance-to-Digital Converter", AN-1585 Application Note, Analog Devices

However, one limitation is that the extension factor is based on a sample by sample basis. Either the baseline reading of the sensor determines the extension factor ($\frac{C_{baseline}}{17pF}$) or the dynamic range of the sensor ($\frac{C_{dynamic}}{8pF}$). Since the sensors are handmade and each has a different baseline, linearity and gauge factor (and thus dynamic range), it

requires constant switching of resistors R_1 and R_2 for different sensors and are not convenient for use. Extension with a large factor to fit all sensors will result in low resolution for short sensors (low baseline reading) or sensors that have a smaller gauge factor (small dynamic range).

Sample data collected with this method is shown in Figure.41:

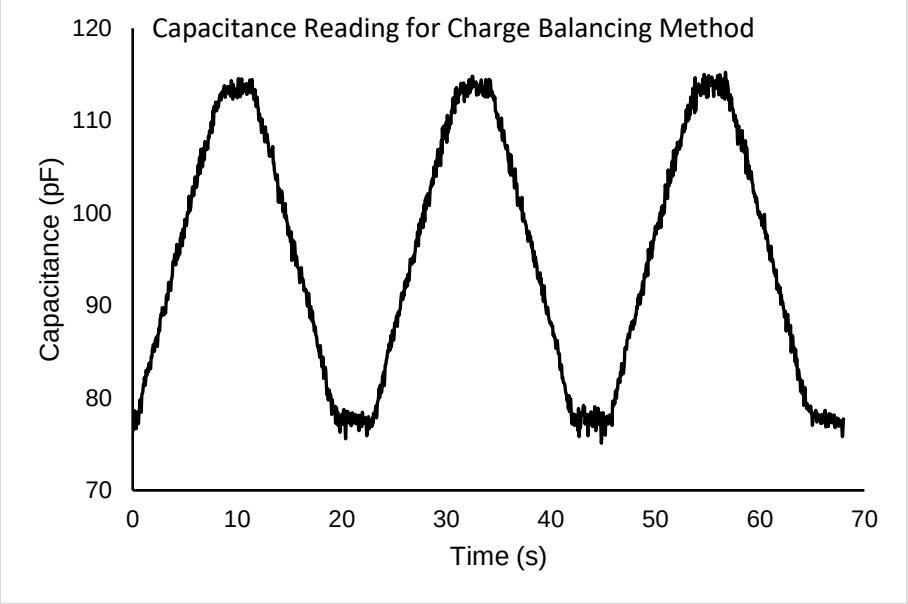

Figure 40 - Sensor data captured by the AD7745

A 50mm sample was subjected to 10% strain trapezoidal wave with a 3 second hold at each maximum/minimum. The range extension was not completed specifically for the tested sample and resulted in an amplification of capacitance amplitude because of the shifted baseline (bulk capacitance) and a changed dynamic range which resulted in calculation errors, but the reading will cap out for larger strain due to insufficient range for the particular sample used.

4.4. 555 Timer Astable Multivibrator Circuit

The 555 timer is a simple, cheap and widely popular chip in timing applications. When configured to its astable multivibrator mode, it can generate a square wave with a variable duty cycle and variable frequency depending on component values in the circuit shown Figure.42

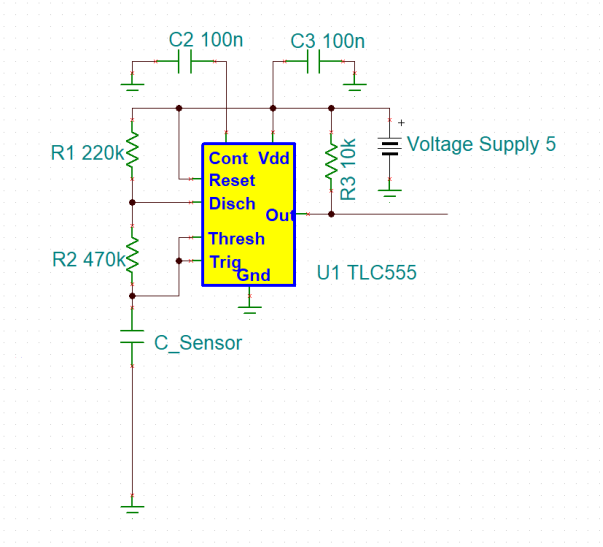

Figure 41 - 555 Timer Astable Multivibrator Circuit

The frequency of the output square wave depends on the capacitance being measured C_{sensor} and the two resistors R_1 and R_2. The capacitance being measured will be charged to 2/3 supply voltage through R_1 and R_2 and discharged to 1/3 supply voltage through R_2. The output square wave will be high during the charging cycle and low during the discharge cycle. The frequency f_{out} of the output wave can be fed to a microcontroller or a counter to be measured.

For this experiment, the output frequency was fed to a microcontroller (Arduino Uno) to trigger interrupts and a counter was incremented by one in the Interrupt Service Routine, a fixed time window to get counter value and reset counter is used to calculate the average frequency

$$f_{out} = \frac{counter\ output}{t_{integration}}$$

The time window functions as a moving average filter and reduces the noise in the signal obtained, a longer time window will produce more stable result than that of a short time window, but the trade-off was the sampling frequency.

With f_{out}, R_1 and R_2 known, capacitance of the sensor can be calculated with the formula:

$$f_{out} = \frac{1}{\ln 2 \times (R_1 + 2 \times R_2) \times C_{sensor}}$$

It is worth noting that despite the sensor has a kOhm equivalent series resistance and seen by both the charge and discharge cycle, the selection of larger R1 and R2 combined with the frequency averaging method resulted in very little noise in the final reading.

Sample data collected with the 555 timer astable multivibrator circuit for a sensor subjected to a repeated triangular wave strain is shown in Figure.43

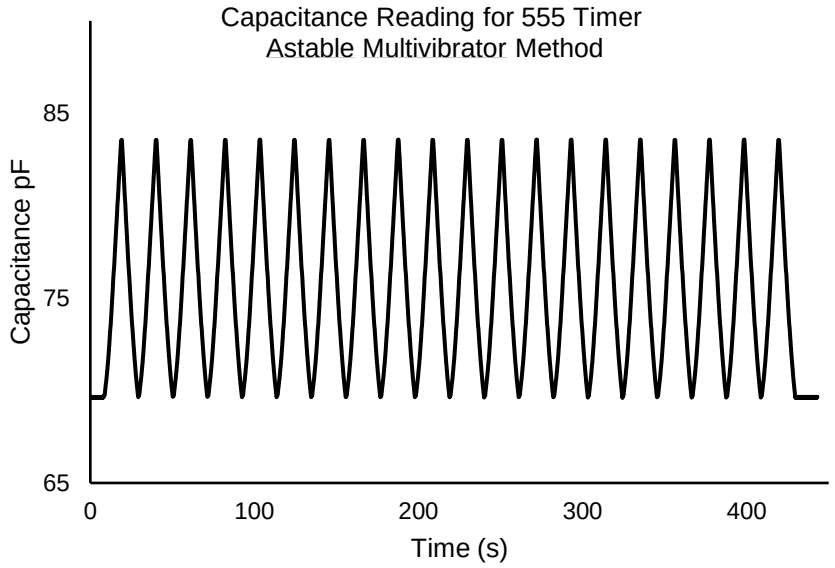

Figure 42 - Sensor capacitance captured by the 555 Timer Astable Multivibrator circuit

The data was collected on a sample sensor subjected to 20 cycles of 25% strain with a triangular wave pattern. The reading had very little noticeable noise as the result of the 100ms integration window used in this test (10 samples/second) and the stable output frequency of the TLC555 timer circuit used.

4.5. Chapter Conclusion

In total 4 types of capacitance measurement circuit were explored, and the strengths and weaknesses are tabulated in Table.1

Table 1 - Advantages and Disadvantages of the explored capacitance measurement circuits

Measurement Method	Advantage	Disadvantage

DC Direct Charge Method	Fast Sampling Rate (100Hz+) Minimal number of components needed in circuit	Highly susceptible to noise Moderate ESR effect on performance
LC Tank Oscillation Method	1. Low Noise 2. Fast Sampling Rate (100Hz+) 3. Single IC solution available	1. Performance severely affected by large equivalent series resistance
Charge Balancing Method	1. Fast sampling rate 2. Minimal performance effect from equivalent series resistance 3. Single IC solution available	1. Requires extension for range to fit different sensors 2. Varying baseline and gauge factor leads to challenges in range extension.
555 Timer Astable Multivibrator Method	1. Minimal noise 2. Simple circuitry with few components	1. Large capacitance will cause output to drop in frequency, affecting maximum sampling frequency 2. Low sampling frequency needed to ensure good noise performance

The equivalent series resistance is not likely to be fully eliminated in the production process, the LC tank oscillation method is not suitable for the soft capacitive strain sensors produced in this study. For the charge balancing AD7745 circuit, its disadvantage can be solved if the production method can be improved to produce sensors with consistent baseline capacitance and consistent gauge factor. A fixed range extension would mean the AD7745 chip will be able to measure full-range capacitance of the sensor at a relatively high frequency (90Hz+) with acceptable noise level (approximately $\pm 0.5pF$ depending on the extension factor). For this study, the 555 Timer Astable Multivibrator method is chosen to be the best suitable capacitance measurement circuit for the current sensor prototypes for its stable reading with minimal noise and this addresses Objective 2 of this thesis. The 555 Timer circuit was used in capacitance data collection for the walking test and produced reliable results that achieved a 99% accuracy in angle prediction.

Chapter 5. Characterization of Improved Sensor

5.1. Improved Capacitive Sensing Filament

Although the previous sensor prototype has repeatable readings that achieved satisfactory performance in the prototype knee brace experiment, there are areas that can be improved. The limitations of the dip-coating apparatus and the dip coating procedure caused the sensor to have an irregular shape in the sensing region that results in non-linear behavior and a relatively low baseline capacitance that ranges from 50pF to 120pF for a 50mm sample (10-24pF/cm). An improved version of the sensor was made for enhanced linearity and higher baseline and is characterized in this chapter.

The main problem faced by the prototype sensor was that the long exposure to the dipping solution because of the slow dip and draw speed of the syringe pump caused applied layers to re-dissolve and crack resulting in an uneven surface and irregular shape. The new protocol used a combination of two dielectric materials (Hytrel 3078 and SEBS) and a combination of hand and machine dipping (syringe pump). 7% weight-volume Hytrel 3078 solution is prepared with dichloromethane, and 10% SEBS weight-volume is prepared with cyclohexane. After applying the inner electrode, a single layer of SEBS was coated with the prepared solution using machine dipping (slow), and then a single layer of Hytrel 3078 was coated on the SEBS through hand dipping with a fast draw speed. Efforts were made to maintain an even draw speed when hand dipping. Then another layer of SEBS was machine dip coated outside of the Hytrel layer. The three-layer dielectric was noticeably thinner than the prototype (prototype diameter 650+um, improved diameter 500um) and also had a higher relative permittivity as the result of adding Hytrel 3078. The resulting sensor samples exhibited high baseline readings of 150-200pF for a 40mm sample (37.5~50pF/cm).

5.2. Characterization

Unless otherwise specified, all the characterizations completed in this chapter have linear displacement patterns and data provided by an Instron Tensile Tester (Instron E10000) and capacitance reading taken by a Precision LCR Meter (Keysight E4980A) and logged by a MatLab script running on a PC.

5.2.1. Stress-Strain Curve

A tensile test was performed on a 40mm improved sensor sample and a 40mm bare extruded Hytrel 3078 filament, the samples were subjected to a 60% linear strain starting from 0% strain at a strain rate of 10%/s. The filaments were connected to the loadcell such that the loadcell reading was barely above 0 when filaments were at 0 strain. The bare extruded Hytrel 3078 filament had a diameter of 420um, and the coated improved sample had a diameter of 500um, assuming the material used is incompressible and isotropic, the cross-section area under strain can be calculated by:

$$A = \frac{\pi {r_0}^2}{1 + \varepsilon}$$

Where r_0 is the initial radius of the filaments, ε is the strain. Then stress can be calculated with the load cell reading F:

$$Stress = \frac{F}{A}$$

The resulting Stress-Strain comparison is plotted in Figure.44

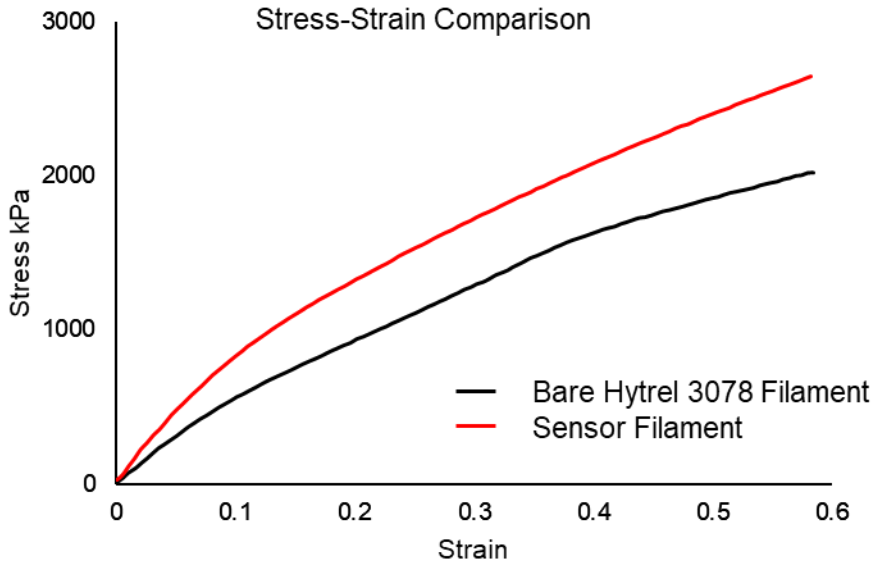

Figure 43 - Stress-strain comparison of bare Hytrel 3078 filament and the coated sensor

It is worth noting that despite having a 50% Carbon Black loading in its electrode layer that lead to a significant amount of reinforcing, the thin (approximately 10um thick) electrodes did not hinder the mechanical performance of the sensor by a significant amount. The elastic region was determined to be approximately 30%.

5.2.2. Large Strain Test

A 34.89mm improved sensor sample was subjected to 100% strain at 1% strain/second. The sensor signal is shown in Figure.45

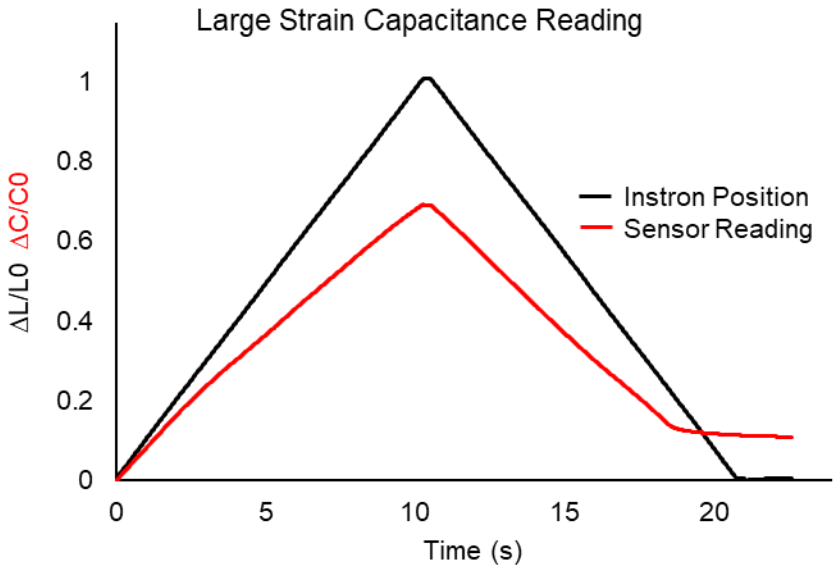

Figure 44 - Sensor reading in large 100% strain showing considerable plastic deformation

The 100% increase in strain resulted a 70% increase in the sensor's reading from its baseline. The gauge factor of this sample can be calculated as:

$$GF = \frac{\Delta C/C_0}{\Delta L/L_0} = \frac{0.7}{1.0} = 0.7$$

With the applied strain ε, theoretical change in sensor length is

$$L = (\varepsilon + 1)L_0$$

where L_0 is the initial length of the sensor and the radii of the sensor's dielectric layer would change to

$$r = \frac{r_0}{\sqrt{\varepsilon + 1}}$$

Substitute the above equations into the cylindrical capacitance equation to obtain the change in capacitance:

$$C = (\varepsilon + 1)L_0 \frac{2\pi\epsilon\epsilon_0}{\ln(\frac{r_{outer_0}}{r_{inner_0}})} = (\varepsilon + 1)C_0$$

The theoretical gauge factor was hence calculated to be 1. The deviation of the sample's gauge factor from 1 could be explained by the potential uneven surface because of the hand dipping procedure, and also by the decreasing dielectric property of the dielectric material under applied strain as reported in [48]. The decrease in slope of the signal suggested a gauge factor that is strain dependent, although for strain smaller than 30% the slope of signal change was more linear, suggesting a constant gauge factor for low strain and an ideal working range of 30% strain.

5.2.3. Hysteresis Curve

A 42.33mm sample is subjected to 5%, 10%, 15%,20%, 25%, 30% strain each repeated for 3 cycles. Sensor signal is plotted against the strain to obtain a hysteresis loop as shown in Figure.46

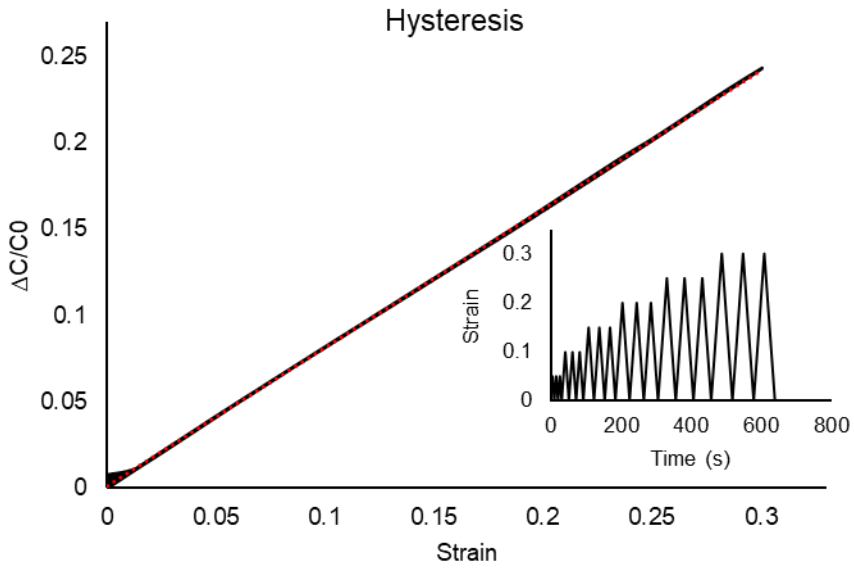

Figure 45 – Hysteresis Curve for the improved sensor in its 30% strain linear region

The high resilience of the sensor core material Hytrel 3078 resulted in very small differences in signal between the load and unload cycles. The sample filament recovers more than 99% of its baseline capacitance value after every cycle. A 1% drift of the base line was observed during the 30% strain cycles as the sensors were not preconditioned. Preconditioning is a process where repeated cycles of 40% strain is used to prepare the sensor for usage for within 30% strain (induced plastic deformation). A simple linear fit was performed on the data and the R2 value is 0.9999 which indicates superior linearity of the sensor signal. It is worth noting also the sensor has a constant gauge factor of approximately 0.81 within the linear operating range. The gauge factor can only be constant within a linear region (gauge factor decreased at higher strain to 0.7) and a constant gauge factor is useful in estimating sensor reading and in calibration.

5.2.4. Frequency Performance

Human motor functions can reach the frequency of 10Hz [64] , it is desirable to test the sensor's signal under fast strain rate and high frequency motion. A 40.07mm sample was prestrained to 10%, and then subjected to a 10% amplitude sinusoidal wave at frequencies 0.1Hz, 1Hz, 10Hz, 15Hz, 20Hz each repeated for 10 cycles. However, there was a limitation to this test. The precision LCR meter used for data collection had a maximum sampling frequency of approximately 50Hz, for higher frequencies, the chance

of the sampled point falling on the peak and valley become increasing low and the full amplitude of the waveform is hard to observe. The collected data is shown in Figure.47

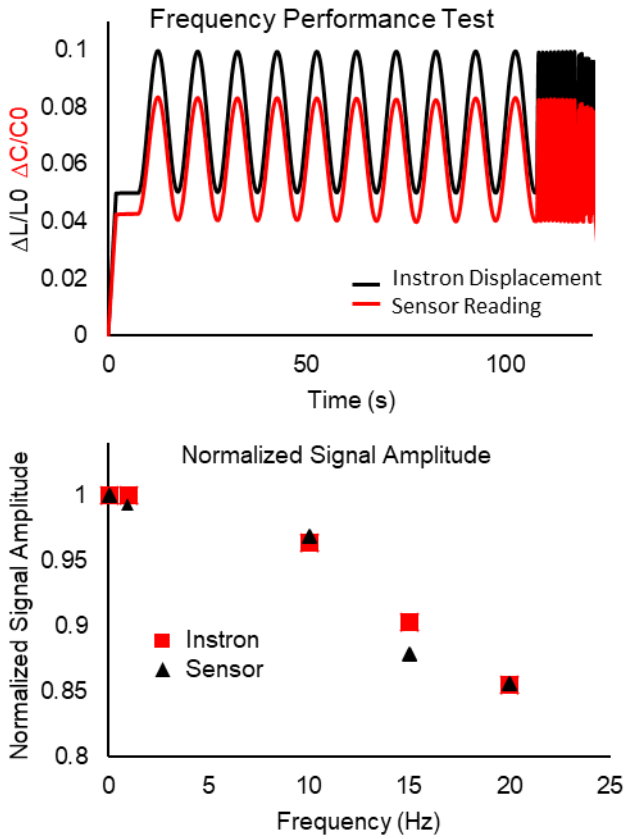

Figure 46 **Top: Sensor Reading for different frequencies**
Bottom: Maximum peak-peak amplitude reached in each frequency band

The Instron tensile tester also experienced some displacement error as frequency increases as shown in the top graph with a decrease in sinusoidal amplitude. A method was proposed to salvage the data by finding a maxima (highest peak sampled) and minima (lowest valley sampled) for each frequency band and calculate the maximum amplitude recorded for that frequency. The same process was performed for both sensor reading and for the Instron displacement amplitude and is graphed in Figure.47 bottom. The sensor capacitance showed the correct number of peaks and valleys and the maximum amplitude of each frequency band correlates to the decrease in the displacement amplitude of the Instron at 0.1, 1, 10, 20Hz. At 15Hz, none of the recorded datapoints was in proximity to the peak/valley of the waveform because of the low number of datapoints per stroke, leading to an error between signal amplitudes.

5.2.5. Long-term Cyclic Stability

To examine material fatigue, a 42.33mm sample was subjected to a 10% of pre-strain and then 1000 sinusoidal cycles with 5% strain. The resulting sensor reading is shown in Figure.48

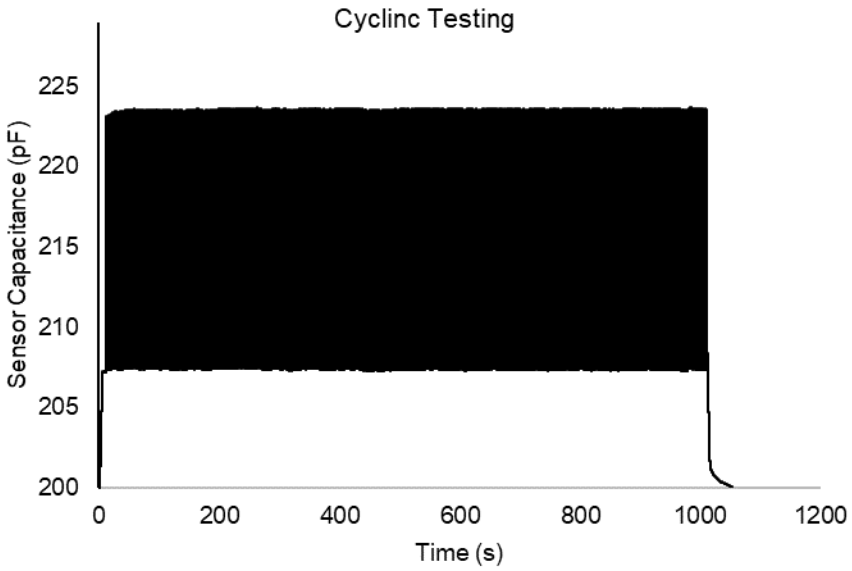

Figure 47 - Cyclic testing for sensor repeatability and material fatigue

The Instron took approximately 30 cycles to reach its full amplitude. Average reading from the 31st to 50th cycle and the last 20 cycle were compared, and the final 20 cycles had an average reading 0.06pF (0.03%) higher than the average reading of the first 20 cycles. Repeatability during cyclic testing is important in real-life motion monitoring applications as repeated motions can potentially cause material fatigue. A 0.03% increase in baseline after 1000 cycles shows good fatigue resistance and promising performance for the purpose of long-term joint movement monitoring.

5.2.6. Static Load

A 42.33 mm sample was subjected to a step-up and step-down pattern with a 5 second hold at 10%, 20% and 30%, the sensor signal is given in Figure.49

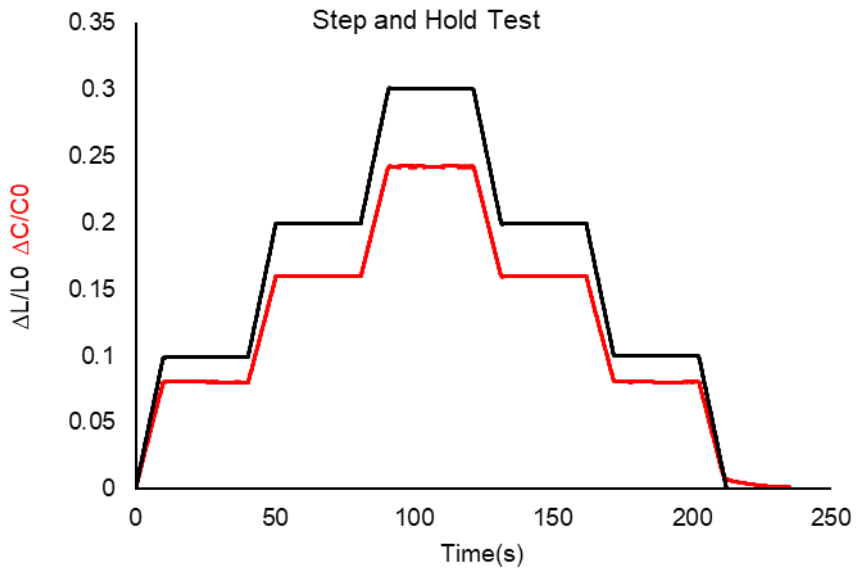

Figure 48 - Sensor reading in step-up and step-down static load test

Capacitance reading held steady during the hold with no noticeable drift except a noise level of $\pm 0.01\%$. This incremental load and unload can be used as the baseline for a linear fit that can be used to predict tensile tester gripper position (or sample length).

5.2.7. Random Tracking

Many researches on soft strain sensors, whether resistive or capacitive often focuses on performance during regular movement such as repeated cycles of a sinusoidal or triangular displacement. But both sensors' performances will stabilize over repeated cycles as reported in [60] as a result of dynamic change in orientation and aggregation of the conductive particle in the sensor. To mimic real world movement, which is almost always random, a continuous random tracking test was performed. A random set of waypoints are fed to the Instron tensile tester and the gripper follows a spline curve through these random waypoints. The readings of the sensor are passed through the previous linear predictor obtained from the previous static load test to predict the position of the gripper. The predicted result was compared with the actual position in the Figure.50:

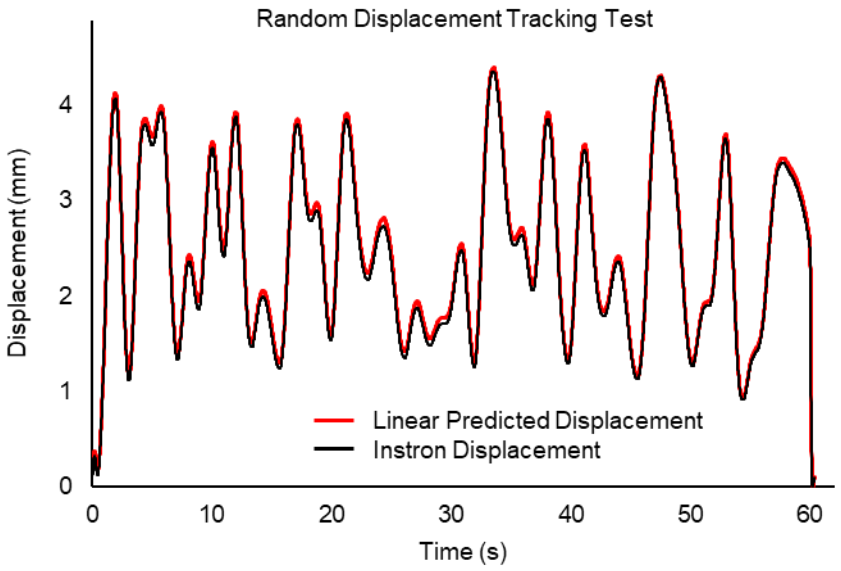

Figure 49 - Sensor predicted displacement compared to reference displacement logged by Instron tensile tester

The RMSE between actual and predicted position is calculated to be 0.06mm, which is 0.14% of the baseline length. The high accuracy is the result of the shielded tensile tester (Instron) and the coaxial cables used in testing and was significantly more accurate than the walking test. For outdoor usage of the sensor, the conductive thread used for embedding the sensor needs to be coaxially shielded cables and the electronic readout circuits should be shielded as well.

5.3. Chapter Conclusion

This chapter addressed objective 1 on the thesis. A downsized soft capacitive strain sensing filament was produced that has a large base capacitance compared to previously reported sensors in the literature (up to 10 times larger), the sensor also exhibits superior linearity with R^2 value of 0.9999 which was also higher than any previously reported sensors although this could be due to the fact that all tests were performed within the elastic region. The drift error under static load was negligible at 0.01% that is better with previously reported values of 0.3% for a similar strain [2]. The baseline capacitance can reach as high as 210pF for a 4 cm sample with 500um diameter, that is higher than the 174pF reported for an 80mm*100mm*0.1mm sample [2] but with a fraction of its size. The cyclic stability test showed a 0.03% increase in reading

after 1000 cycles and was better than the reported 0.38% increase after 1000 cycles of 40% strain reported in [54].

Chapter 6. Conclusion

6.1. Conclusion

The original objectives of the thesis and the current accomplishment is tabulated in Table.2

Table 2 - Objectives and Accomplishment

Objectives		Accomplishment
To develop a reliable capacitive filament sensor that has…	low drift under static load with less than 0.1% change in reading	Drift during the static loading test showed 0.01% variations in the reading
	good cyclic performance with less than 0.3% change in readings after 1000 cycles	Cyclic testing showed 0.03% increase in reading after 1000 cycles.
	good linearity within the elastic region R^2>0.9995 [44]	Readings show a linear relationship to applied strain with a R^2 value of 0.9999
	large baseline reading >150pF to provide good signal-to-noise ratio	Sensors produced show a capacitance of 37.5-50pF/cm, the upper bound of 50pF/cm can easily be reached by controlling hand-dipping speed.
To develop reliable circuitry for data collection		Experimented on different types of data collection circuit, analyzed their strengths and decided on using the 555 Astable Multivibrator circuit as the data collection circuit for the walking tests. Signal quality was good and required little preprocessing to achieve satisfactory result in fitting/prediction
To perform real-time monitoring of knee angle with the sensor embedded in garments. Achieve 96% [49] accuracy when compared with video-based motion capture system.		With a simple calibration method, sensor was able to predict knee angle accurate to 1% of the baseline angle with a simple computational model.
Simple calibration protocol for real life usage		Calibration achieved with analog goniometer (protractor) without the involvement of training sessions and trial runs. The calibration method provided the accuracy needed for the study and took less than 5 minutes.

6.2. Limitation

Despite the satisfactory performance of the current prototype, it is not without its limitations. The readout circuit suffers from low sampling rate because of the requirement of a long enough integration period to produce stable readings. While it is enough to capture normal motion, high frequency human motion typically presented in Parkinson patients with tremor might be a challenge as the readout circuitry used in this study cannot support a high enough sampling rate. The combination of a high equivalent series resistance that result from the sensor electrode and their piezoresistive behaviour under strain prevents usage of some frequency-based ICs that can provide higher sampling rate. The production method of the improved filament involves human error during the step of hand dipping. While the best effort was made to draw with a steady hand at constant speed. This procedure can be improved through the use of a proper dip-coating machine. The current embedding method, while robust, exerts large compressional force on the sensor lead because of the hammered-on metal snap buttons. Although this compression will not affect the sensing area, it can potentially result in material fatigue and breakage at the connection point.

6.3. Future Work

With the current material selection, a non-solvent approach is preferred where the material is melt mixed with carbon black and then coextruded by a micro-co-extruder to achieve the desirable dimension and layer thickness, the tubular shape will then allow a single micro-coaxial cable to be connected on one end to collect reading in a more noise-resistant manner.

Unlike resistive sensors where machine learning algorithms are needed to compensate for the sensor reading quality, the computational power offered by modern machine learning algorithms can be redirected to establish a model-less approach where a redundant array of the capacitive strain sensing filament can be used to monitor more complicated motions for joints with more than one degree of freedom such as the shoulder and the wrist. A mesh weaved by the capacitive sensing filament can also be used to reconstruct a 3D topology of complex surfaces with the help of deep learning when the surface are put face down on the mesh, deforming the mesh because of gravity.

Bibliography

[1] M. Amjadi, Y. J. Yoon, and I. Park, “Ultra-stretchable and skin-mountable strain sensors using carbon nanotubes–Ecoflex nanocomposites,” *Nanotechnology*, vol. 26, no. 37, p. 375501, Sep. 2015.

[2] A. Atalay *et al.*, “Batch Fabrication of Customizable Silicone-Textile Composite Capacitive Strain Sensors for Human Motion Tracking,” *Advanced Materials Technologies*, vol. 2, no. 9, p. 1700136, 2017.

[3] O. Atalay, “Textile-Based, Interdigital, Capacitive, Soft-Strain Sensor for Wearable Applications,” *Materials*, vol. 11, no. 5, p. 768, May 2018.

[4] O. Atalay, A. Atalay, J. Gafford, H. Wang, R. Wood, and C. Walsh, “A Highly Stretchable Capacitive-Based Strain Sensor Based on Metal Deposition and Laser Rastering,” *Advanced Materials Technologies*, vol. 2, no. 9, p. 1700081, Sep. 2017.

[5] S. Bahadori, T. Immins, and T. W. Wainwright, “A review of wearable motion tracking systems used in rehabilitation following hip and knee replacement,” *Journal of Rehabilitation and Assistive Technologies Engineering*, vol. 5, p. 2055668318771816, 2018.

[6] A. Bîrcă, O. Gherasim, V. Grumezescu, and A. M. Grumezescu, “Introduction in thermoplastic and thermosetting polymers,” in *Materials for Biomedical Engineering*, Elsevier, 2019, pp. 1–28.

[7] “Bîrcă et al. - 2019 - Introduction in thermoplastic and thermosetting po.pdf.” .

[8] L. Cai *et al.*, “Super-stretchable, Transparent Carbon Nanotube-Based Capacitive Strain Sensors for Human Motion Detection,” *Scientific Reports*, vol. 3, p. 3048, Oct. 2013.

[9] H. Cao *et al.*, “Development and Characterization of a Novel Interdigitated Capacitive Strain Sensor for Structural Health Monitoring,” *IEEE Sensors Journal*, vol. 15, no. 11, pp. 6542–6548, Nov. 2015.

[10] Y. Cha, H. Kim, and D. Kim, “Flexible Piezoelectric Sensor-Based Gait Recognition,” *Sensors (Basel)*, vol. 18, no. 2, Feb. 2018.

[11] T. Chen *et al.*, “Analysis of the gyro misalignment angle in Goniometer based on fiber optic gyroscope,” *Optik*, vol. 127, no. 2, pp. 769–772, 2016.

[12] C. Choi, J. M. Lee, S. H. Kim, S. J. Kim, J. Di, and R. H. Baughman, “Twistable and Stretchable Sandwich Structured Fiber for Wearable Sensors and Supercapacitors,” *Nano Letters*, vol. 16, no. 12, pp. 7677–7684, Dec. 2016.

[13] J. Choi and K. Hong, “3D skin length deformation of lower body during knee joint flexion for the practical application of functional sportswear,” *Applied Ergonomics*, vol. 48, pp. 186–201, May 2015.

[14] D. J. Cohen, D. Mitra, K. Peterson, and M. M. Maharbiz, “A Highly Elastic, Capacitive Strain Gauge Based on Percolating Nanotube Networks,” *Nano Lett.*, vol. 12, no. 4, pp. 1821–1825, Apr. 2012.

[15] C. B. Cooper *et al.*, “Stretchable Capacitive Sensors of Torsion, Strain, and Touch Using Double Helix Liquid Metal Fibers,” *Advanced Functional Materials*, vol. 27, no. 20, p. 1605630, May 2017.

[16] T. de Oliveira Sato, G.-Å. Hansson, and H. J. C. G. Coury, “Goniometer Crosstalk Compensation for Knee Joint Applications,” *Sensors (Basel)*, vol. 10, no. 11, pp. 9994–10005, Nov. 2010.

[17] J. Eom *et al.*, “Highly Sensitive Textile Strain Sensors and Wireless User-Interface Devices Using All-Polymeric Conducting Fibers,” *ACS Applied Materials & Interfaces*, vol. 9, no. 11, pp. 10190–10197, Mar. 2017.

[18] Y. Fan, C. Liao, L. Xie, and X. Chen, “Piezo-capacitive behavior of a magnetically structured particle-based conductive polymer with high sensitivity and a wide working range,” *Journal of Materials Chemistry C*, vol. 6, no. 20, pp. 5401–5411, 2018.

[19] G. Ferriero, S. Vercelli, F. Sartorio, and C. Foti, “Accelerometer-based goniometer for smartphone and manual measurement on photographs: do they agree?,” *Biomedizinische Technik. Biomedical engineering*, vol. 59, no. 6, pp. 549–550, 2014.

[20] A. Filippeschi, N. Schmitz, M. Miezal, G. Bleser, E. Ruffaldi, and D. Stricker, “Survey of Motion Tracking Methods Based on Inertial Sensors: A Focus on Upper Limb Human Motion,” *Sensors*, vol. 17, no. 6, p. 1257, Jun. 2017.

[21] A. S. Fiorillo, C. D. Critello, and S. A. Pullano, “Theory, technology and applications of piezoresistive sensors: A review,” *Sensors and Actuators A: Physical*, vol. 281, pp. 156–175, Oct. 2018.

[22] A. Frutiger *et al.*, “Capacitive Soft Strain Sensors via Multicore–Shell Fiber Printing,” *Advanced Materials*, vol. 27, no. 15, pp. 2440–2446, 2015.

[23] A. Frutiger *et al.*, “Sensors: Capacitive Soft Strain Sensors via Multicore–Shell Fiber Printing (Adv. Mater. 15/2015),” *Advanced Materials*, vol. 27, no. 15, pp. 2548–2548, Apr. 2015.

[24] O. Glauser, D. Panozzo, O. Hilliges, and O. Sorkine-Hornung, “Deformation Capture via Soft and Stretchable Sensor Arrays,” *ACM Trans. Graph.*, vol. 38, no. 2, pp. 1–16, Mar. 2019.

[25] A. D. Gray *et al.*, “Development and Validation of a Portable and Inexpensive Tool to Measure the Drop Vertical Jump Using the Microsoft Kinect V2,” *Sports Health*, vol. 9, no. 6, pp. 537–544, Dec. 2017.

[26] C. Guger, B. Allison, F. Cao, and G. Edlinger, “A Brain-Computer Interface for Motor Rehabilitation With Functional Electrical Stimulation and Virtual Reality,” *Archives of Physical Medicine and Rehabilitation*, vol. 98, no. 10, pp. e24–e24, 2017.

[27] G.-A. Hansson, I. Balogh, K. Ohlsson, and S. Skerfving, “Measurements of wrist and forearm positions and movements: effect of, and compensation for, goniometer crosstalk,” *J Electromyogr Kinesiol*, vol. 14, no. 3, pp. 355–367, Jun. 2004.

[28] J. Ho, T. R. Jow, and S. Boggs, “Historical introduction to capacitor technology,” *IEEE Electrical Insulation Magazine*, vol. 26, no. 1, pp. 20–25, Jan. 2010.

[29] M. Khoshnam, D. M. C. Häner, E. Kuatsjah, X. Zhang, and C. Menon, “Effects of Galvanic Vestibular Stimulation on Upper and Lower Extremities Motor Symptoms in Parkinson’s Disease,” *Front. Neurosci.*, vol. 12, 2018.

[30] S.-R. Kim, J.-H. Kim, and J.-W. Park, “Wearable and Transparent Capacitive Strain Sensor with High Sensitivity Based on Patterned Ag Nanowire Networks,” *ACS Appl. Mater. Interfaces*, vol. 9, no. 31, pp. 26407–26416, Aug. 2017.

[31] G. Kofod, H. Stoyanov, and R. Gerhard, “Multilayer coaxial fiber dielectric elastomers for actuation and sensing,” *Appl. Phys. A*, vol. 102, no. 3, pp. 577–581, Mar. 2011.

[32] M. Kollosche, H. Stoyanov, S. Laflamme, and G. Kofod, “Strongly enhanced sensitivity in elastic capacitive strain sensors,” *J. Mater. Chem.*, vol. 21, no. 23, pp. 8292–8294, May 2011.

[33] A. A. Mohamed, J. Baba, J. Beyea, J. Landry, A. Sexton, and C. A. McGibbon, “Comparison of strain-gage and fiber-optic goniometry for measuring knee kinematics during activities of daily living and exercise,” *J Biomech Eng*, vol. 134, no. 8, p. 084502, Aug. 2012.

[34] J. Mou *et al.*, “Uncertainty analysis of dynamic goniometer based on fiber optic gyroscope,” 2019, vol. 10839, pp. 108391T–108391T–9.

[35] J. T. Muth *et al.*, “Embedded 3D Printing of Strain Sensors within Highly Stretchable Elastomers,” *Advanced Materials*, vol. 26, no. 36, pp. 6307–6312, 2014.

[36] R. Nur, N. Matsuhisa, Z. Jiang, M. O. G. Nayeem, T. Yokota, and T. Someya, “A Highly Sensitive Capacitive-type Strain Sensor Using Wrinkled Ultrathin Gold Films,” *Nano Lett.*, vol. 18, no. 9, pp. 5610–5617, Sep. 2018.

[37] R. A. Ouckama, “Comparison of Flexible Electrogoniometers to a 3 D Optical Tracking System for Measurements of Ankle Angles During Level Walking and Running,” 2008.

[38] J. Park, I. You, S. Shin, and U. Jeong, “Material Approaches to Stretchable Strain Sensors,” *ChemPhysChem*, vol. 16, no. 6, pp. 1155–1163, 2015.

[39] A. Ravve, “Principles of Polymer Chemistry,” *Principles of Polymer Chemistry*, 1995.

[40] S. Rosset and H. R. Shea, “Flexible and stretchable electrodes for dielectric elastomer actuators,” *Appl. Phys. A*, vol. 110, no. 2, pp. 281–307, Feb. 2013.

[41] R. Sarban, R. W. Jones, B. R. Mace, and E. Rustighi, “A tubular dielectric elastomer actuator: Fabrication, characterization and active vibration isolation,” *Mechanical Systems and Signal Processing*, vol. 25, no. 8, pp. 2879–2891, Nov. 2011.

[42] T. Sekitani, Y. Noguchi, K. Hata, T. Fukushima, T. Aida, and T. Someya, “A Rubberlike Stretchable Active Matrix Using Elastic Conductors,” *Science*, vol. 321, no. 5895, pp. 1468–1472, Sep. 2008.

[43] S. Seyedin *et al.*, “Textile strain sensors: a review of the fabrication technologies, performance evaluation and applications,” *Mater. Horiz.*, vol. 6, no. 2, pp. 219–249, 2019.

[44] J. Shintake, E. Piskarev, S. H. Jeong, and D. Floreano, “Ultrastretchable Strain Sensors Using Carbon Black-Filled Elastomer Composites and Comparison of Capacitive Versus Resistive Sensors,” *Advanced Materials Technologies*, vol. 3, no. 3, p. 1700284, 2018.

[45] S. Son and N. C. Goulbourne, “Finite Deformations of Tubular Dielectric Elastomer Sensors,” *Journal of Intelligent Material Systems and Structures*, vol. 20, no. 18, pp. 2187–2199, Dec. 2009.

[46] S. Stassi, V. Cauda, G. Canavese, and C. F. Pirri, “Flexible Tactile Sensing Based on Piezoresistive Composites: A Review,” *Sensors*, vol. 14, no. 3, pp. 5296–5332, Mar. 2014.

[47] H. Stoyanov, M. Kollosche, S. Risse, R. Waché, and G. Kofod, “Soft Conductive Elastomer Materials for Stretchable Electronics and Voltage Controlled Artificial Muscles,” *Advanced Materials*, vol. 25, no. 4, pp. 578–583, 2013.

[48] V. L. Tagarielli, R. Hildick-Smith, and J. E. Huber, “Electro-mechanical properties and electrostriction response of a rubbery polymer for EAP applications,” *International Journal of Solids and Structures*, vol. 49, no. 23–24, pp. 3409–3415, Nov. 2012.

[49] M. Totaro *et al.*, “Soft Smart Garments for Lower Limb Joint Position Analysis,” *Sensors*, vol. 17, no. 10, p. 2314, Oct. 2017.

[50] B. N. M. Truong and K. K. Ahn, “Modeling and control of hysteresis for DEAP actuator,” *Sensors and Actuators A: Physical*, vol. 201, pp. 193–206, Oct. 2013.

[51] S. Vercelli, F. Sartorio, E. Bravini, and G. Ferriero, “DrGoniometer: a reliable smartphone app for joint angle measurement,” *Br J Sports Med*, vol. 51, no. 23, pp. 1703–1704, Dec. 2017.

[52] L. Vilhena and A. Ramalho, “Friction of Human Skin against Different Fabrics for Medical Use,” *Lubricants*, vol. 4, no. 1, p. 6, Mar. 2016.

[53] T. Vu-Cong, C. Jean-Mistral, and A. Sylvestre, “Impact of the nature of the compliant electrodes on the dielectric constant of acrylic and silicone electroactive polymers,” *Smart Mater. Struct.*, vol. 21, no. 10, p. 105036, Sep. 2012.

[54] H. Wang *et al.*, “Downsized Sheath–Core Conducting Fibers for Weavable Superelastic Wires, Biosensors, Supercapacitors, and Strain Sensors,” *Advanced Materials*, vol. 28, no. 25, pp. 4998–5007, 2016.

[55] S. Wang, P. Wang, and T. Ding, “Resistive viscoelasticity of silicone rubber/carbon black composite,” *Polymer Composites*, vol. 32, no. 1, pp. 29–35, 2011.

[56] T. Wang, R. Wang, Y. Cheng, and J. Sun, “Quasi In Situ Polymerization To Fabricate Copper Nanowire-Based Stretchable Conductor and Its Applications,” *ACS Appl. Mater. Interfaces*, vol. 8, no. 14, pp. 9297–9304, Apr. 2016.

[57] M. A. Watkins, D. L. Riddle, R. L. Lamb, and W. J. Personius, “Reliability of goniometric measurements and visual estimates of knee range of motion obtained in a clinical setting,” *Phys Ther*, vol. 71, no. 2, pp. 90–96; discussion 96-97, Feb. 1991.

[58] E. L. White, M. C. Yuen, J. C. Case, and R. K. Kramer, “Low-Cost, Facile, and Scalable Manufacturing of Capacitive Sensors for Soft Systems,” *Advanced Materials Technologies*, vol. 2, no. 9, p. 1700072.

[59] C. Xu, J. He, X. Zhang, X. Zhou, and S. Duan, “Towards Human Motion Tracking: Multi-Sensory IMU/TOA Fusion Method and Fundamental Limits,” *Electronics*, vol. 8, no. 2, p. 142, Jan. 2019.

[60] K. Yamaguchi, J. J. C. Busfield, and A. G. Thomas, “Electrical and mechanical behavior of filled elastomers. I. The effect of strain,” *Journal of Polymer Science Part B: Polymer Physics*, vol. 41, no. 17, pp. 2079–2089, 2003.

[61] S. Yao *et al.*, “Silver nanowire strain sensors for wearable body motion tracking,” in *2015 IEEE SENSORS*, 2015, pp. 1–4.

[62] M. Yazdifar, M. R. Yazdifar, J. Mahmud, I. Esat, and M. Chizari, “Evaluating the Hip Range of Motion Using the Goniometer and Video Tracking Methods,” *Procedia Engineering*, vol. 68, pp. 77–82, 2013.

[63] X. You *et al.*, “Stretchable capacitive fabric electronic skin woven by electrospun nanofiber coated yarns for detecting tactile and multimodal mechanical stimuli,” *J. Mater. Chem. C*, vol. 6, no. 47, pp. 12981–12991, Dec. 2018.

[64] H. Zeng and Y. Zhao, “Sensing Movement: Microsensors for Body Motion Measurement,” *Sensors*, vol. 11, no. 1, pp. 638–660, Jan. 2011.

[65] W. Zhao, M. A. nthal, D. D. Espy, and X. Luo, “Rule-Based Human Motion Tracking for Rehabilitation Exercises: Realtime Assessment, Feedback, and Guidance,” *IEEE Access*, vol. 5, pp. 21382–21394, 2017.

[66] Z. Zhao, C. Shuai, Y. Gao, E. Rustighi, and Y. Xuan, “An application review of dielectric electroactive polymer actuators in acoustics and vibration control,” *J. Phys.: Conf. Ser.*, vol. 744, p. 012162, Sep. 2016.

[67] “Capacitor Model.” [Online]. Available: http://www.iequalscdvdt.com/cap_model.html. [Accessed: 06-Nov-2019].

[68] “Goniometer vs. Motion Capture Measurement in Physical Therapy,” *EuMotus*. [Online]. Available: https://www.eumotus.com/post/goniometer-vs-motion-capture-measurement-in-physical-therapy. [Accessed: 05-Nov-2019].

[69] “Twin-Axis Electrogoniometers for Joint Movement Analysis.” [Online]. Available: http://www.biometricsltd.com/goniometer.htm. [Accessed: 10-Nov-2019].

[70] Smooth-On Inc, “Silicone Rubber – Platinum Cure,” EcoFlex datasheet, December, 2018 .

[71] Smooth-On Inc, “Silicone Rubber – Platinum Cure,” DragonSkin datasheet, December, 2018 .

[72] DuPont, “Thermoplastic Polyester Elastomer,” Hytrel 3078 datasheet, Feb. 2014 [Revised Oct. 2005].

[73] Arkema, “Thermoplastic Polyether Block Amide,” Pebax 3533 datasheet

[74] Analog Devices, “24-Bit Capacitance-to-Digital Converter with Temperature Sensor,” AD7745 datasheet[Revised Apr. 2005].

[75] Texas Instrument, “FDC2114 and FDC2214 EVM User’s Guide”, FDC2214EVM datasheet, June 2015. [Revised October 2016]